MULTI-SENSOR BASED AMBIENT ASSISTED LIVING SYSTEM

A THESIS

SUBMITTED TO THE DEPARTMENT OF ELECTRICAL AND

ELECTRONICS ENGINEERING

AND THE GRADUATE SCHOOL OF ENGINEERING AND SCIENCE

OF BILKENT UNIVERSITY

IN PARTIAL FULFILLMENT OF THE REQUIREMENTS

FOR THE DEGREE OF

MASTER OF SCIENCE

By

Ahmet Yazar

July, 2013

I certify that I have read this thesis and that in my opinion it is fully adequate, in scope and in quality, as a thesis for the degree of Master of Science.

Prof. Dr. A. Enis Çetin (Advisor)

I certify that I have read this thesis and that in my opinion it is fully adequate, in scope and in quality, as a thesis for the degree of Master of Science.

Prof. Dr. Billur Barshan

I certify that I have read this thesis and that in my opinion it is fully adequate, in scope and in quality, as a thesis for the degree of Master of Science.

Assoc. Prof. Dr. İbrahim Körpeoğlu

Approved for the Graduate School of Engineering and Science:

Prof. Dr. Levent Onural
Director of the Graduate School

ABSTRACT

MULTI-SENSOR BASED AMBIENT ASSISTED LIVING SYSTEM

Ahmet Yazar
M.S. in Electrical and Electronics Engineering
Supervisor: Prof. Dr. A. Enis Çetin
July, 2013

An important goal of Ambient Assisted Living (AAL) research is to contribute to the quality of life of the elderly and handicapped people and help them to maintain an independent lifestyle with the use of sensors, signal processing and the available telecommunications infrastructure. From this perspective, detection of unusual human activities such as falling person detection has practical applications. In this thesis, a low-cost AAL system using vibration and passive infrared (PIR) sensors is proposed for falling person detection, human footstep detection, human motion detection, unusual inactivity detection, and indoor flooding detection applications. For the vibration sensor signal processing, various frequency analysis methods which consist of the discrete Fourier transform (DFT), mel-frequency cepstral coefficients (MFCC), discrete wavelet transform (DWT) with different filter-banks, dual-tree complex wavelet transform (DT-$\mathbb{C}$WT), and single-tree complex wavelet transform (ST-$\mathbb{C}$WT) are compared to each other to obtain the best possible classification result in our dataset. Adaptive-threshold based Markov model (MM) classifier is preferred for the human footstep detection. Vibration sensor based falling person detection system employs Euclidean distance and support vector machine (SVM) classifiers and these classifiers are compared to each other. PIR sensors are also used for falling person detection and this system employs two PIR sensors. To achieve the most reliable system, a multi-sensor based falling person detection system which employs one vibration and two PIR sensors is developed. PIR sensor based system has also the capability of detecting uncontrolled flames and this system is integrated to the overall system. The proposed AAL system works in real-time on a standard personal computer or chipKIT Uno32 microprocessors without computers. A network is setup for the communication of the Uno32 boards which are connected to different sensors. The main processor gives final decisions and emergency alarms are transmitted to outside of the smart home using the auto-dial alarm system

via telephone lines. The resulting AAL system is a low-cost and privacy-friendly system thanks to the types of sensors used.

Keywords: Ambient assisted living, vibration sensor, passive infrared sensor, complex wavelet transform, support vector machines, falling person detection, Markov models, human footstep detection, unusual inactivity detection, indoor flooding detection.

ÖZET

ÇOKLU ALGILAYICI TABANLI ÇEVRE DESTEKLİ YAŞAM SİSTEMİ

Ahmet Yazar
Elektronik ve Elektronik Mühendisliği, Yüksek Lisans
Tez Yöneticisi: Prof. Dr. A. Enis Çetin
Temmuz, 2013

Çevre destekli yaşam araştırmalarının amacı, yaşlı ve bakıma muhtaç kişilerin yaşam kalitelerine katkıda bulunabilmektir. Algılayıcıların, işaret işleme yöntemlerinin ve halihazırdaki iletişim altyapısının kullanılmasıyla bu kişiler için özgür bir yaşam biçimi sağlanabilecektir. Bu bakış açısıyla, düşen kişi örneği gibi olağandışı insan hareketlerinin tespit edilebilmesinin kullanışlı uygulamaları bulunmaktadır. Bu tezde, titreşim ve pasif kızılberisi algılayıcıları kullanılarak düşük maliyetli bir çevre destekli yaşam sistemi önerilmiştir. Alt sistemler; düşen kişi tespiti, insan adımı tespiti, hareket/hareketsizlik tespiti ve bina içi su taşkını tespiti uygulamalarından oluşmaktadır. Titreşim algılayıcının frekans içeriğinden öznitelik çıkarımı yapabilmek için ayrık Fourier dönüşümü, mel-frekansı kepstral katsayıları, ayrık dalgacık dönüşümü, çift ağaç karmaşık dalgacık dönüşümü ve tek ağaç karmaşık dalgacık dönüşümü yöntemleri veri kümemiz üzerinde en iyi sınıflandırma sonucunu sağlayabilmek için birbirleriyle karşılaştırılmıştır. İnsan adımı tespiti için, uyarlanabilir eşik değerli Markov modelleri sınıflandırıcısı tercih edilmiştir. Titreşim algılayıcı tabanlı düşen kişi tespiti uygulamasında Euclidean uzaklığı ve destek vektör makineleri sınıflandırıcıları kullanılmıştır. Bu sınıflandırıcı yöntemlerinin aralarında karşılaştırma yapılmıştır. İki tane pasif kızılberisi algılayıcı aynı anda kullanılarak farklı bir düşen kişi tespiti yaklaşımı geliştirilmiştir. Sonrasında, titreşim algılayıcı ve iki tane pasif kızılberisi algıyacısının birlikte kullanıldığı daha güvenilir bir düşen kişi tespiti uygulaması tanıtılmıştır. Daha önceki çalışmalardan olan kontrolsüz alev tespiti sistemi, çevre destekli akıllı ev tasarımına dahil edilmiştir. Önerilen sistem gerçek zamanlı olarak standart bir bilgisayarda ya da chipKIT Uno32 mikroişlemciler üzerinde çalışabilmektedir. Her bir algılayıcıya bağlı Uno32 işlemciler için bir ağ kurularak işlemcilerin haberleşmeleri sağlanmıştır. Ana işlemci tüm kararları birleştirerek sonuçta oluşacak muhtemel bir acil durum alarmını telefon hatları üzerinden evin

dışındaki istenen bir merkeze iletebilmektedir. Bu amaçla otomatik aramalı alarm sistemi geliştirilmiştir.

Anahtar sözcükler: Çevre destekli yaşam, titreşim algılayıcı, pasif kızılberisi algılayıcı, karmaşık dalgacık dönüşümü, destek vektör makineleri, düşen kişi tespiti, Markov modelleri, insan adımı tespiti, hareketsizlik tespiti, bina içi su taşkını tespiti.

Acknowledgement

I would like to express my gratitude to my supervisor Prof. Dr. A. Enis Çetin for his guidance, encouragement, and useful comments and remarks throughout the development of this thesis.

Furthermore, I would like to offer my special thanks to Prof. Dr. Billur Barshan and Assoc. Prof. Dr. İbrahim Körpeoğlu for accepting to read and review this thesis.

I wish to thank Osman Günay for his great help in solving many problems. Thanks to Furkan Keskin for sharing his ST-$\mathbb{C}$WT works and his friendship.

I would also like to thank Kıvanç Köse who have willingly shared his precious time whenever I need to consult him. I would also like to thank İhsan İnaç for sharing his knowledge about the hardwares used in this work.

My thanks are extended to Onur Yorulmaz, Serdar Çakır, Oğuzcan Dobrucalı, Necip Gürler, Akın Sevimli, and Alexander Suhre for their collaboration and constructive friendship.

I would like to specially thank Hasan Hüseyin Erkaya who supported me all the way through my undergraduate years at Eskişehir. He has become and is more than a teacher for me.

I would like to acknowledge valuable support of my mother whose warm-hearted and encouraging spirit always refreshed me, and my father whose I feel his firm support always with me.

Besides, I am grateful that Information and Communication Technologies Authority has given me opportunity to complete this thesis.

I would also like to express my appreciation to TÜBİTAK for providing scholarship (BİDEB-2210) throughout my graduate study.

This work was supported by Türk Telekom under Grant Number 3015-03.

Contents

List of Figures

List of Tables

Chapter 1

Introduction

Most European countries including Turkey will face a large increase in the number of elderly people in the near future. The development of intelligent homes will improve the quality of life of seniors and the handicapped people. As a result, a lot of studies are introduced to improve intelligent homes in the last ten years. It is possible to use different sensors to improve the quality of the elderly people's lives.

It is reported that unexpected falling is a major problem and about one-third of people over 65 falls unexpectedly each year [1]. Fall related health and injury costs are on the order of billions of dollars worldwide. Additionally, unusual inactivity detection is also very important because of the sudden diseases like heart attacks. As a result, we focus on the falling person detection systems and decided that an ambient assisted living (AAL) system can be designed using vibration and PIR sensors for this purpose. This thesis presents a multi-sensor based AAL system which has the capability of falling person detection, human footstep detection, human motion detection, unusual inactivity detection, indoor flooding detection and uncontrolled flame detection. Correspondingly, various frequency analysis methods, different classifiers, and novel algorithms related with the subsystems are described. The main aim of the overall system is to transmit an alarm whenever an emergency situation happens in the elderly person's house.

1.1 Related Work

There are several different types of smart home designs in the literature [2]. Computer vision systems can be used to track the person and classify his/her movements in a house [3], [4]. In recent years, the number of the Kinect sensor based systems continue to increase for the smart home implementations [5], [6]. Wearable devices are often used in similar applications [7], [8], [9], [10]. There are also several different types of sensor network based systems in the literature [11], [12], [13], [14].

The available smart home applications can be categorized in two main groups: Ambient assisted systems and wearable systems. Ambient systems include computer vision based systems, Kinect sensor based systems, and different types of sensor network based systems [15]. Wearable systems are based on accelerometers, miniature inertial and magnet sensors [7], [8], [9], [10]. Computer vision based systems have generally low miss-detection rates and high number of false alarms because of the abundance of information in video processing. However, most people find having a camera in their houses invasion of their privacy, even if the video and sound recordings are not transmitted elsewhere. Also, the computer vision based systems need high computational power of processors and large number of cameras to handle blind spots. Additionally, there is a certain installation cost of the computer vision based system so the overall system can be defined as a high-cost system. Kinect sensor based systems have almost the same conditions with the computer vision based systems [4], [6], [15]. They are thought as more privacy friendly systems than the computer vision based systems but they are not completely privacy-friendly systems.

Currently, there are many available commercial products which are based on the wearable devices. The wearable systems have remarkable advantages. For example, these systems do not need any installation cost and there is only one module which is placed on the person. However, the main disadvantage of these systems is that wearing and/or carrying them is not convenient all the time and elderly people may simply forget to put on these sensors.

Lastly, advantages and disadvantages of the sensor network based systems can vary accordingly to the sensor types and the number of the used sensors. Our vibration sensor and PIR sensor based system's advantages are privacy-friendly, unnoticeable system to the person, only one-dimensional signal processing, and the system does not have a wearable component. The large number of the sensors and the certain installation cost can be considered as the disadvantages of our sensor network based system.

There are many other studies in the subsystem areas of our AAL system. The related works are examined for each of the detection systems one by one. As a start, a survey paper about principles and approaches for the falling person detection is published last year [15]. It is accepted that fall detection systems help elderly people to maintain an independent way of life [16], [17]. Currently, the commercially available fall detection systems feature body-worn sensors which are connected to a wireless network [18], [9]. There are other recent studies which turn a mobile phone into a fall detector [19]. Computer vision and Kinect sensor based fall detectors are studied in various works [4], [6], [15]. Vibration sensor based fall detection systems are proposed in two studies so far [20], [21]. However, pattern recognition algorithms for fall detection are not described in the mentioned articles. Without a recognition algorithm the resulting system will not be a robust and practical system. There are also multi-PIR-sensor based fall detectors which use generally more than four PIR sensors [22], [23].

Human footstep or walking person detection is another application studied using different hardwares. Computer vision based systems can be used in mobile systems like pedestrian detection by a camera system in the car [24]. Vibration sensor or seismic sensor based systems are used indoor and outdoor widely [25], [26]. Also, human footstep detection systems can be employed in the military applications [27]. Detection of the daily physical activities using a tri-axial accelerometer is another working area for the similar subjects [28]. Additionally, unusual inactivity detection systems are implemented using computer vision based and belt-worn kinematic sensor based systems [29], [30]. As a last subsystem, indoor flooding detection applications generally use simple low-cost sensors however there are also some computer vision based systems [31].

In the theoretical part of the thesis, various frequency analysis methods including the discrete wavelet transform (DWT) and the dual-tree complex wavelet transform (DT-$\mathbb{C}$WT) are studied. The DT-$\mathbb{C}$WT has recently emerged as a promising alternative to the classical DWT [32]. The DT-$\mathbb{C}$WT has desirable properties such as shift-invariance and lack of aliasing however it still suffers from increased data rate in the transform domain. Several versions of the DT-$\mathbb{C}$WT are proposed in the literature for reducing the computational complexity of the transform [33]. In [34], rational coefficient filters are designed and employed in lattice and lifting structures for efficient implementation of the DT-$\mathbb{C}$WT however, dual-tree structure is retained. In [35], the authors propose a single-tree complex wavelet transform utilizing complex-valued filter-banks in the tree for face recognition, but this approach introduces complex arithmetic and it increases the amount of data as in the DT-$\mathbb{C}$WT.

1.2 Contribution

One of the contributions of this thesis is the design of a *real* single-tree lifting-based wavelet transform that possesses complex wavelet-like characteristics, such as near shift-invariance and lack of aliasing. Unlike [34] in which dual-tree approach is used, we design a single-tree lifting-based complex wavelet transform. Our filter-bank has time-varying update and prediction filters for lifting structures in the single-tree context. Time-varying nature of the proposed filters enables the implementation of half-sample delayed filters in a single tree in an interchangeable manner.

Our system is different from the currently available AAL systems. We propose to install both vibration and PIR sensors to an intelligent home to realize a robust system. These two different types of sensors complement each other and daily activities of seniors can be monitored without producing false alarms and unusual events like falling can be reliably detected. The resulting AAL system will be a low-cost and privacy-friendly system thanks to the types of sensors used.

Human footstep detection is succeed by using the adaptive-threshold based Markov model (MM) classifier. More importantly, three separate falling person detection algorithms are introduced in this thesis, and all of these falling person detection algorithms are novel. Also, the stand-alone AAL system using the vibration and two PIR sensors is described as an original study.

1.3 Thesis Outline

In Chapter 2, the microprocessor unit for the real-time system, the vibration sensor, the PIR sensor and the auto-dial alarm system via telephone lines are described. Various frequency analysis methods which consist of the DFT, MFCC, DWT, DT-$\mathbb{C}$WT, and ST-$\mathbb{C}$WT are introduced in Chapter 3. In Chapter 4, the subsystems of our AAL system, classification methods and experimental setups are described. Chapter 5 is the last chapter that concludes the thesis by providing an overall summary of the results and gives some ideas for the future works.

Chapter 2

Hardware Implementations

Sensor-based AAL systems can contain different equipments. These equipments may have various advantages and disadvantages. For a multi-sensor based smart home application, the system designer should take into account the characteristics of these individual components meticulously. In this chapter, sensors and other complementary components which we employed in the AAL system are described.

In Section 2.1, the microprocessor unit for the real-time system is introduced. Analog-to-digital conversion and other processes are all done on these microprocessor units. Vibration sensor and an analog-front-end circuit are described in Section 2.2. One-axis vibration sensor is used to sense vibrations on the floor. The PIR sensor and a modified sensor circuit are described in Section 2.3. PIR sensors are generally used in human motion detection based applications. Microcontroller-compatible auto-dial alarm system is presented in Section 2.4. Our auto-dial alarm system transmits the desired emergency alarms to a call center or to an operator via telephone lines.

2.1 Arduino Prototyping Platform

Arduino is a prototyping platform based on easy-to-use hardware and software [36]. All of the hardware and software are open-source for the Arduino protoyping platforms. There are several Arduino boards for different purposes. One of the modest one is Arduino Uno board. This electronics board is modernized by Digilent Inc. and chipKIT Uno32 board is developed as an Arduino-compatible platform. The Uno32 combines Arduino compatibility with the Microchip PIC32 microcontroller. 26.95 USD chipKIT Uno32 board is shown in Figure 2.1. The Uno32 electronics board has the following properties [37]:

- Microchip PIC32MX320F128H microcontroller (80 MHz 32-bit MIPS, 128K Flash, 16K SRAM),
- Compatible with many existing Arduino code samples and other resources,
- Arduino Uno form factor,
- Compatible with many Arduino shields,
- 42 available I/O pins,
- Two user LEDs,
- PC connection uses a USB A > mini B cable,
- 12 analog inputs (10-bit resolution ADC),
- 3.3 V operating voltage,
- 80 MHz operating frequency,
- 75 mA typical operating current,
- 7 V to 15 V input voltage,
- 0 V to 3.3 V analog input voltage range,
- +/−18 mA DC current per pin.

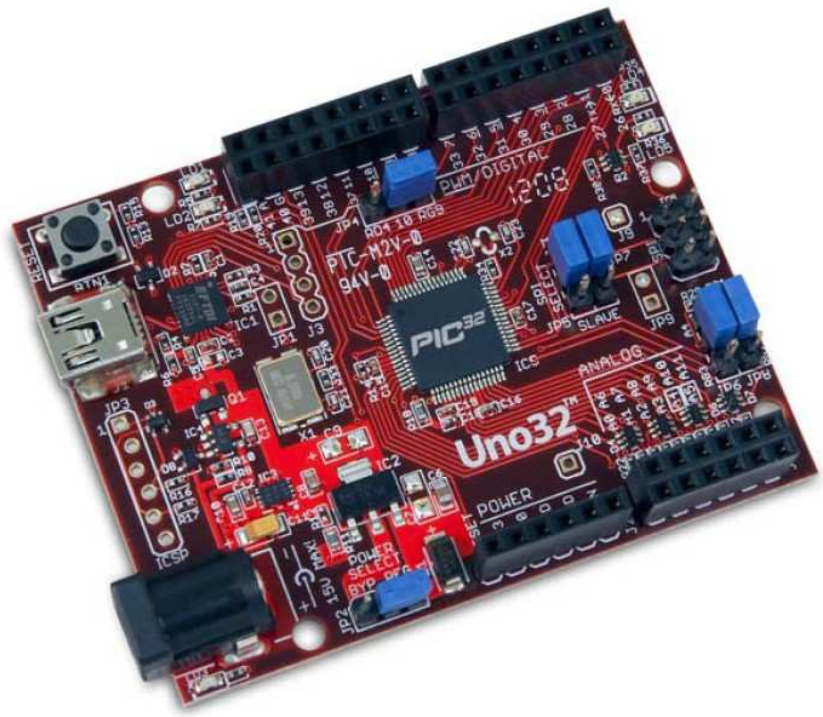

Figure 2.1: chipKIT Uno32 board.

The Arduino programming language is based on C/C++. Arduino IDE or Digilent's own IDE can be used to program the chipKIT boards. Digilent Inc. develops MPIDE (Multi Platform Integrated Development Environment) which is a modified version of the Arduino IDE. MPIDE is compatible with Digilent's boards and native Arduino boards. We used MPIDE to program the chipKIT Uno32 board.

The Uno32 board is employed as an analog-to-digital converter while developing algorithms with MATLAB on a personal computer. Analog signals of the vibration and PIR sensors are digitized with 8-bit resolution using the Uno32 board. Next, all algorithms are implemented on the Uno32 board without a personal computer. An auto-dial alarm module also works compatible with the microcontrollers including Arduino boards. The overall AAL system is implemented as a stand-alone project quite easily thanks to the chipKIT Uno32 prototyping platform.

2.2 The Vibration Sensor

Vibration sensors are also called as a seismic sensor, seismometer or geophone. In literature, "seismic" and "geophone" words are generally used in the geophysics-related articles. In this thesis, we prefer "vibration" instead of "seismic" and "geophone" to prevent possible misunderstandings.

We employ the vibration sensor with the aim of sensing the vibrations on the floor. The vibration sensor converts vibrations into electrical signals depending on the intensity of the vibration waves in the axis of the vibration sensor.

Vibration sensors can be categorized into two groups based on the number of their axes: One-axis and three-axis sensor types. We used one-axis vibration sensor in this thesis to analyze vibrations in up-down axis.

2.2.1 Sensor Properties

Schematics presentation of internal structure of the vibration sensor is presented in Figure 2.2. The vibration sensor is basically formed by a sensing coil, springs, and a fixed magnet. The sensing coil moves in up-down axis with the help of springs when there is a vibration. While the coil moves along an axial magnetic field provided by a fixed magnet, an electrical signal is produced in direct proportion to the intensity of the vibration waves [38]. The bottom of the vibration sensor must be in contact with the floor to convert vibrations into electrical signals.

In this thesis, we used a GS-20DX vibration sensor which is manufactured by OYO Technologies. This sensor can detect vibration signals from distances up to 25 meters. The height, the diameter, and the weight of the GS-20DX vibration sensor are 3.30 cm, 2.54 cm, and 87.3 g, respectively. Its price is about 25.00 USD.

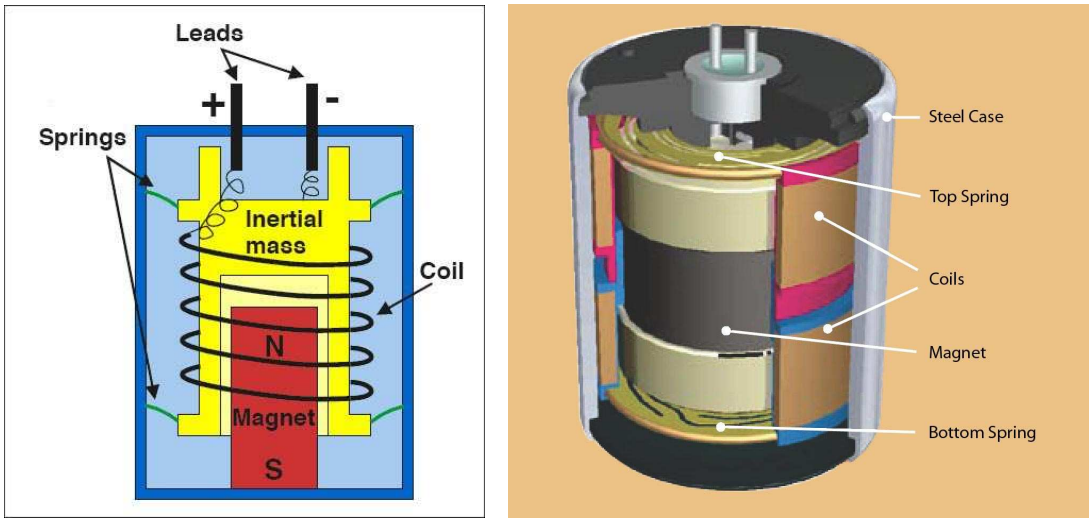

(a) (b)

Figure 2.2: Schematics presentations of internal structures of different vibration sensors. The left figure (a) is taken from [38], and the right figure (b) is taken from [39].

2.2.2 Related Work

There are several different studies related with vibration sensors. Footstep detection applications have an important place in these studies [40], [41], [42]. The aim of the footstep detection is generally related with security applications and military missions. Vibration sensors are suitable for these tasks because they can be hidden easily and they do not need a viewing angle to sense the environment.

Vibration sensors are used in the classification of pistachio nuts and their kernels [43]. In these types of works, sensor model should be selected as more sensitive to impact. Another study is about classification of vehicles [44]. As it is seen from vibration sensor based applications, vibration sensors have a wide range of usage by different industries. Everything generates vibration while moving. Therefore, vibration sensors may be used to classify movement activities.

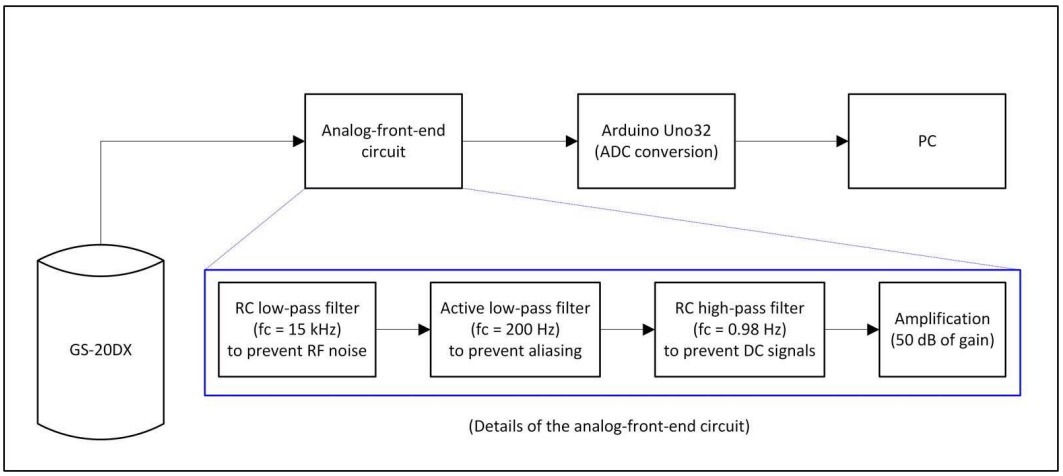

Figure 2.3: Stages of the vibration sensor signal processing.

2.2.3 Sensor Signal Processing

A GS-20DX vibration sensor does not contain any filtering and amplification circuits. The vibration sensor produces a very small electrical voltage. Therefore, output signal of the vibration sensor needs to be filtered and amplified before further signal processing operations.

An analog-front-end circuit is implemented inspired by the analog circuit example in [41]. Our circuit contains an RC low-pass filter ($f_c = 15$ kHz) to prevent RF noise, an active low-pass filter ($f_c = 200$ Hz) to prevent aliasing, and a RC high-pass filter ($f_c = 0.98$ Hz) to prevent DC signals. At the last stage, amplification is done with 50 dB of gain in 0-2.5 V voltage range. All filtering and amplification stages are presented in Figure 2.3. The analog-front-end circuit's energy is derived by Arduino Uno32 board's 5 V output.

After reaching an appropriate analog signal, analog-to-digital conversion is implemented. Analog vibration signals are sampled at a rate of 500 Hz and digitized with 8-bit resolution using Arduino Uno32 board. An example vibration sensor signal is presented in Figure 2.4. This is a raw signal without pre-processing. The y axis is proportional to the voltage value of the analog signal.

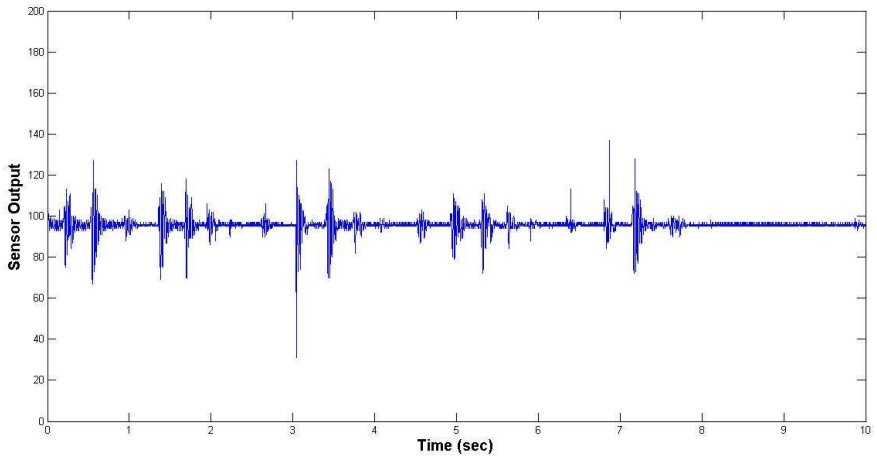

Figure 2.4: 10-second-long vibration sensor signal sample corresponding to a walking event.

2.3 The PIR Sensor

Generally, there are two types of infrared sensors: Active and passive. Active infrared sensors emit infrared radiation and monitor changes in the received power [45]. On the contrary, passive infrared (PIR) sensors only measure infrared radiation, rather than emitting it. In literature, PIR also refers to pyroelectric infrared because most PIR sensors are basically made of pyroelectric materials. In this thesis, we prefer using "passive infrared" instead of "pyroelectric infrared".

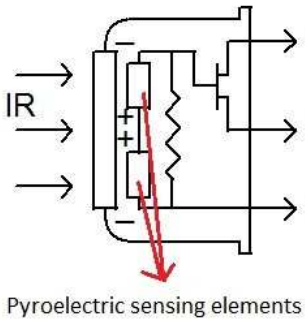

Figure 2.5: Schematics illustration of internal structure of the PIR sensor which contains two reverse-connected pyroelectric sensing elements, taken from [46].

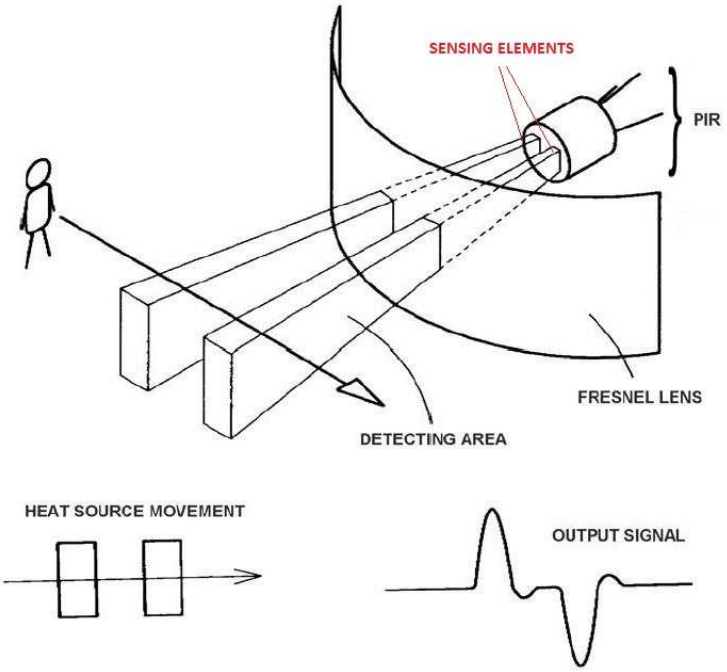

Figure 2.6: An example illustration to describe working mechanism of the PIR sensor, taken from [46].

Objects that generate heat also generate infrared radiation [46]. Every object emits some low level infrared radiation but hotter ones emit more infrared radiation than others. Infrared radiation cannot be seen by human eye but it can be detected by a PIR sensor. PIR sensors work entirely by sensing the infrared radiation emitted by other objects. Generally, PIR sensors are used to sense motion, specially human motion. It should be also pointed out that PID (passive infrared detector) abbreviation is rarely used for the PIR-based motion detectors.

2.3.1 Sensor Properties

Infrared radiation is absorbed by the crystalline material in the PIR sensor and converted to heat [47]. Pyroelectric material in a PIR sensor gives an electrical response to the rate of change in the heat which is related with the rate of change in the infrared radiation.

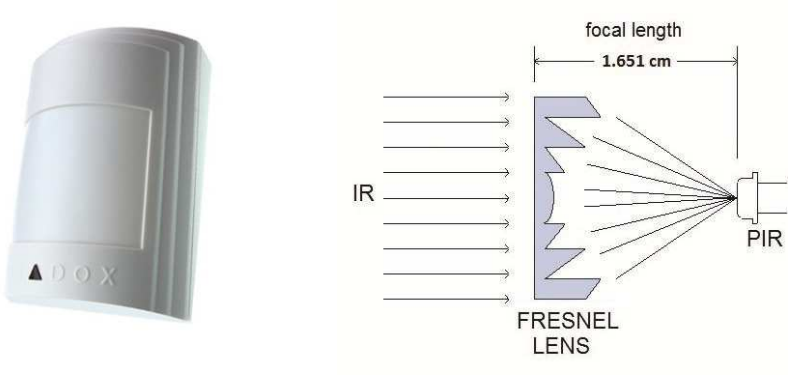

(a) (b)

Figure 2.7: Paradox Pro Plus 476+ (a) and schematics illustration of the Fresnel lens on the detector box (b). The right figure (b) is taken from [46].

PIR sensors usually contain two reverse-connected pyroelectric sensing elements as shown in Figure 2.5. These two sensing elements eliminate the noise caused by vibration, temperature changes and sunlight by producing signals in different directions. For example, if the room temperature changes suddenly, two sensing elements neutralize each other and the output of the PIR sensor remains as a flat signal. The heat source must pass across the PIR sensor in a horizontal direction to activate the sensing elements sequentially as presented in Figure 2.6 [46]. In this way, the strength of the PIR sensor signal is increased by a human motion in the viewing range of the PIR sensor.

In this thesis, Paradox Pro Plus (476+) PIR-based motion detector is used with a simple modification. Modification details are presented in Section 2.3.3. On the outside surface of the detector box, a Fresnel lens is placed to condense the light to provide a larger range of infrared sensing capability to the PIR sensor. Detector box and schematics illustration of the Fresnel lens are shown in Figure 2.7. This Fresnel lens's infrared transmitting material has an infrared transmission range of 8 to 14 μm which is the most sensitive range to human body infrared radiation [46]. The range of the detector is up to 11 meters with 110 $^\circ$ viewing angle as presented in Figure 2.8. The price of Paradox 476+ detector is about 5.00 USD.

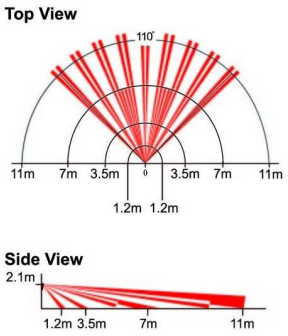

Figure 2.8: Top and side views of the range of PIR sensor, taken from Paradox 476+ datasheet.

2.3.2 Related Work

There are several different studies related with PIR sensors. These studies are generally based on motion detection. Automatic lighting applications are widely used to turn on the lights when motion is detected and turn off the lights when the motion is not detected. Studies for the low power consumption lighter, automatic dimming level adjuster, and automatic room light intensity detector are made in recent years [48], [49], [50]. PIR sensors can be used in various alarm systems for security purposes [51], [52]. Multi-sensor based human localization and tracking applications are developed in [53], [54]. There are also people counting systems implemented using PIR sensor arrays [55], [56].

Some of the other example works are uncontrolled flame detection, gas leak detection, and vehicle monitoring systems [57], [58], [59], respectively. As it is seen, PIR sensor based applications have a wide range of usage for different purposes. Every objects emit some low level infrared radiation. Therefore, PIR sensors can be used to classify motions of different objects which have different heat levels and/or different amount of movements.

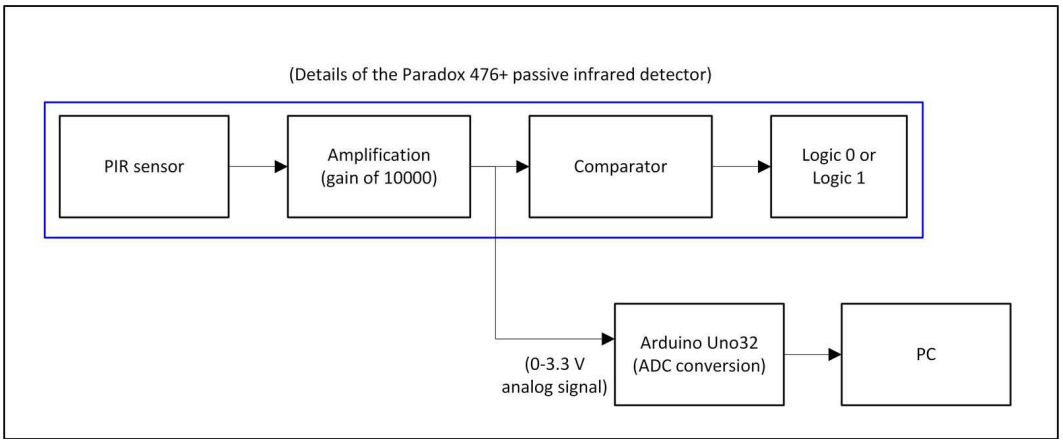

Figure 2.9: Stages of the PIR sensor signal processing.

2.3.3 Sensor Signal Processing

Actually, Paradox 476+ is a PID which gives an output of logical one if there is a human motion activity and an output of logical zero if there is not any motion activity within the viewing range of the PIR sensor. As it can be seen from Figure 2.9, sensor signal is amplified before any operation. After the amplification stage, the signal is converted to pulses and output signal is given as logical zero or logical one. However, using only 1-bit digital signal limits the abilities of the PIR sensor. Therefore, we modified the related circuit and take the output of amplification stage as an analog signal. By this way, we can apply different algorithms to amplified analog PIR sensor signal instead of using 1-bit digital signal.

In this thesis, analog PIR sensor signals are sampled at a rate of 100 Hz and digitized with 8-bit resolution using Arduino Uno32 board. An example PIR sensor signal is presented in Figure 2.10. The y axis is proportional to the voltage value of the analog signal. 12 V DC adapter is used to feed Paradox 476+ PIR-based motion detector.

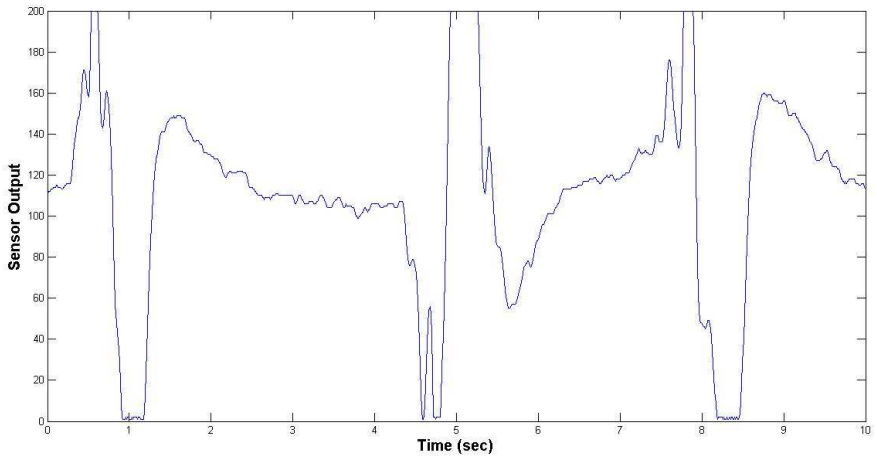

Figure 2.10: 10-second-long PIR sensor signal sample corresponding to a walking event.

2.4 Auto-Dial Alarm System

An auto-dial alarm system is developed to inform emergency units via telephone lines when there is an emergency situation. For example, if there is an uncontrolled flame in the house, the detection system produces an alarm and firefighters are informed automatically by the auto-dial alarm system. As another example, if a falling person is detected in the house, a call center is informed by the auto-dial alarm system. Then, the call center calls the house to confirm the likelihood so that if the phone call is not answered and judgement is made that there is a falling person. Consequently, if the call remains unanswered then, the call center informs the hospital immediately. As it is seen, the auto-dial alarm system is a connector between the house and emergency units.

In our auto-dial alarm system implementation, chipKIT Uno32 and microcontroller-compatible HT9200A DTMF tone generator integrated circuit are used as shown in Figure 2.11. The HT9200A is designed for microcontroller interfaces and it can be instructed by a microcontroller to generate 16 dual and 8 single tones from the DTMF pin. The HT9200A employ a data input, a 5-bit code, and a synchronous clock to transmit a DTMF signal. Every digit of a phone number to be transmitted is selected by a series of inputs which consist of 5-bit

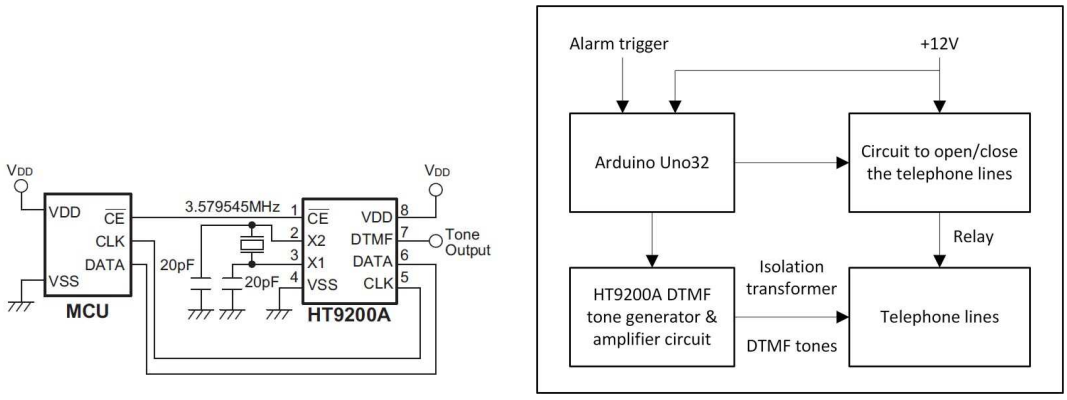

(a) (b)

Figure 2.11: Application circuit for the HT9200A DTMF tone generator (a) and illustration of the auto-dial alarm system (b).

data [60]. A constant phone number is stored and used by the Uno32 board in our tests.

The block diagram of the overall auto-dial alarm system is shown in Figure 2.11 (b). The auto-dial alarm system is triggered by the related detection systems. If there is an emergency situation, the telephone line is turned on by Uno32 board and a simple relay circuit. Meanwhile, Uno32 board also sends the telephone number as bits and HT9200A DTMF tone generator starts to send DTMF tones to the telephone line. HT9200A DTMF tone generator converts the bits into DTMF tones and these tones are amplified before sending to the telephone line. Isolation transformer is used between the tone signals and telephone line because telephone lines have not any reference grounds. Therefore, we need an isolation transformer to provide a reference ground in the system. After the calling the telephone number in a desired duration, the system closes the telephone line.

Different applications can be implemented to understand the reason of an alarm. For example, different telephone numbers can be called for the different emergency situations. Or, ringing times can be varied for the different alarms. Our auto-dial alarm system implementation is presented in Figure 2.12.

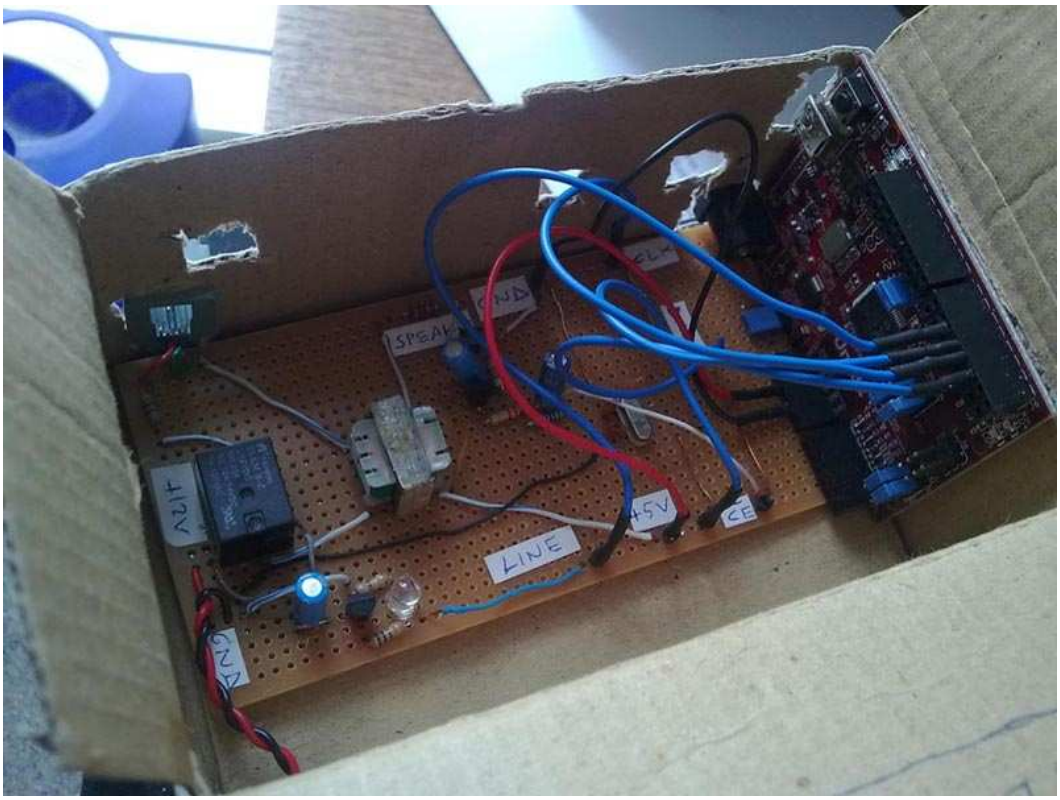

Figure 2.12: Auto-dial alarm system circuit board.

2.5 Summary

In this chapter, sensors and other complementary hardwares employed in our AAL system are described. Arduino-compatible chipKIT Uno32 boards are used to process sensor signals and implement the other control parts of the system. Internal structures and properties of the vibration and PIR sensors are introduced. Microcontroller-compatible auto-dial emergency alarm system is proposed. In the next chapters, theoretical methods and detection algorithms are introduced as a connection between the digitized analog sensor signals and the auto-dial alarm system for land-line telephone systems.

Chapter 3

Feature Extraction from One-Dimensional Signals

In this chapter, different frequency analysis methods from one-dimensional signals are studied and compared to each other. These frequency analysis methods are employed for the vibration sensor signal processing in the next chapter. Discrete Fourier transform (DFT), mel-frequency cepstral coefficients (MFCC), discrete wavelet transform (DWT), and dual-tree complex wavelet transform (DT-$\mathbb{C}$WT) based feature extraction methods are reviewed in Section 3.1. We use $\mathbb{C}$ instead of C for the complex number symbol because C is generally used in the meaning of "continuous" for the CWT abbreviation [61]. In Section 3.2, single-tree complex wavelet transform (ST-$\mathbb{C}$WT) method using time-varying lifting structure is described and compared with the classical methods reviewed in Section 3.1. At the same time, two-second-long vibration sensor signal windows are examined to extract features using these signal analysis methods.

For the DT-$\mathbb{C}$WT, two different filter-banks are executed in parallel to analyze a given input signal, which increases the amount of data after analysis. In the proposed ST-$\mathbb{C}$WT structure, filters of the lifting filter-bank switch back and forth between the two analysis filters of the DT-$\mathbb{C}$WT. This approach does not

increase the amount of output data as the time-varying lifting structure is a critically sampled transform and it has the desirable properties of the DT-$\mathbb{C}$WT such as shift-invariance and lack of aliasing. Shift-invariance properties of the signal analysis methods are compared to each other in Section 3.3. In Section 3.4, computational complexity based comparison between the frequency analysis methods is presented.

3.1 Classical Signal Analysis Methods

Classical frequency analysis methods; DFT, MFCC, DWT, and DT-$\mathbb{C}$WT are employed to analyze frequency content of the vibration sensor signal.

A sample of two-second-long sensor signal and the frequency sub-bands of this signal are presented in Figure 3.1. In this thesis, eight frequency sub-bands are used for the all frequency analysis methods. Boundary frequencies of these sub-bands are $f_s/256$, $f_s/128$, $f_s/64$, $f_s/32$, $f_s/16$, $f_s/8$, $f_s/4$, and $f_s/2$ which correspond to 1.95, 3.91, 7.81, 15.63, 31.25, 62.5, 125, and 250 Hz, respectively, with the sampling frequency $f_s = 500$ Hz. Sub-band energies of the eight frequency sub-bands are computed and used as eight feature parameters for the classification purposes.

It is observed that most of the vibration sensor signal energy is concentrated in low-frequency bands. Hence, more emphasis is given to lower frequencies by assigning more sub-bands to them. For the all frequency analysis methods, the same frequency boundaries are used for the sub-bands so that comparison between the frequency analysis methods can be done more appropriately. Shift-invariance property based comparison and computational complexity based comparison are made between the classical frequency analysis methods and the ST-$\mathbb{C}$WT method in Section 3.3 and 3.4, respectively.

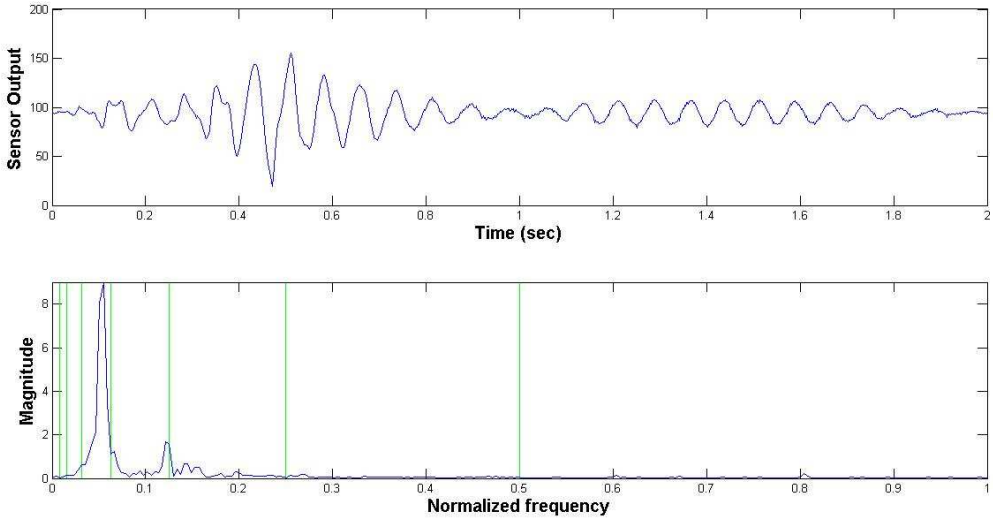

Figure 3.1: DFT of a two-second-long vibration sensor signal record of a falling person and boundary values of the related frequency sub-bands.

3.1.1 Discrete Fourier Transform

The DFT divides the input signal into angular frequency sub-bands [0, $\pi/128$], [$\pi/128$, $\pi/64$], [$\pi/64$, $\pi/32$], [$\pi/32$, $\pi/16$], [$\pi/16$, $\pi/8$], [$\pi/8$, $\pi/4$], [$\pi/4$, $\pi/2$], and [$\pi/2$, π] which correspond to [0, 1.95], [1.95, 3.91], [3.91, 7.81], [7.81, 15.63], [15.63, 31.25], [31.25, 62.5], [62.5, 125], and [125, 250] Hz bands, respectively. As mentioned before, more emphasis is given to lower frequencies by assigning more sub-bands to them. Energy values, $G(m)$, of the eight frequency sub-bands are computed with Eq. 3.1 and used as eight feature parameters:

$$G(m) = \sum_{k \in B(m)} |X(k)|^2 \tag{3.1}$$

where $X(k)$ is the DFT of the input signal and represents the mth frequency band, for $m = 1, \ldots, 8$. For the 1024-point DFT, $B(m)$ represents the indices of sub-band boundaries [1, 4], [5, 8], [9, 16], [17, 32], [33, 64], [65, 128], [129, 256], and [257, 512] for our frequency sub-bands.

3.1.2 Mel-Frequency Cepstral Coefficients

Mel-cepstrum is widely used in speech and image processing [62], [63], [64]. Most of the vibration sensor signal energy is concentrated in low-frequency sub-bands therefore MFCC can be considered as an appropriate candidate for feature extraction from vibration sensor signal because the frequency decomposition of the MFCC is logarithmic giving more emphasis to lower frequencies compared to higher frequencies.

As pointed out in Section 3.1.1 after computation of the DFT of the input signal window, energies of the frequency sub-bands are calculated with Eq. 3.1. Eight feature parameters are extracted by finding eight mel-frequency cepstral coefficients, $C(u)$, with the following formula using the discrete cosine transform (DCT):

$$C(u) = DCT^{-1}\left\{\log\left(G(m)\right)\right\}, u = 1, \ldots, 8 \tag{3.2}$$

The eight mel-frequency cepstral coefficients are used as eight feature parameters for the classification purposes.

3.1.3 Discrete Wavelet Transform

Seven-level DWT is applied to the input signal using one of the wavelets: Haar, Daubechies-2, Daubechies-4, or Biorthogonal-3.3. The Daubechies-4 wavelet has low-pass filter coefficients $h_0[n] = \{0.0106, 0.0329, 0.0308, -0.1870, -0.0280, 0.6309, 0.7148, 0.2304\}$, and high-pass filter coefficients $h_1[n] = \{0.2304, 0.7148, -0.6309, -0.0280, 0.1870, 0.0308, -0.0329, -0.0106\}$.

As shown in Figure 3.2, in a seven-level wavelet tree the sub-signal $x_0[n]$ comes from $[0, \pi/128]$, $x_1[n]$ comes from $[\pi/128, \pi/64]$, $x_2[n]$ comes from $[\pi/64, \pi/32]$, $\ldots$, and $x_7[n]$ comes from $[\pi/2, \pi]$ frequency sub-bands of the input signal $x[n]$, respectively. Feature parameters are extracted by finding the energies of resulting frequency sub-bands. The feature vector for the input signal is defined as follows:

$$v = [\|x_0\|^2 \quad \|x_1\|^2 \quad \ldots \quad \|x_7\|^2]^T. \tag{3.3}$$

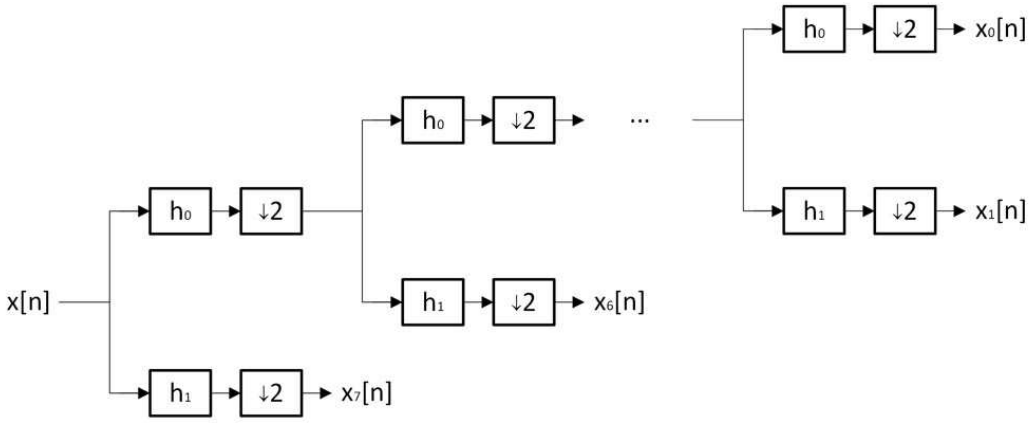

Figure 3.2: Seven-level wavelet tree.

3.1.4 Dual-Tree Complex Wavelet Transform

The DT-ℂWT has recently emerged as a promising alternative to the classical DWT for a variety of signal processing tasks [32]. The classical DWT has several limitations hampering its effectiveness in signal and image analysis, such as time-variance and lack of directionality [61]. It is well-known that the discrete wavelet coefficients may change significantly when the input is shifted slightly. To overcome such limitations of DWT, the DT-ℂWT is proposed whereby two filter pairs are used in parallel to decompose a given signal [65]. In contrast to the real DWT, two sets of filters are employed in the two wavelet trees, which are called real and imaginary trees, respectively. The implementation scheme of a seven-level complex wavelet tree is proposed in Figure 3.3. As it can be seen from this figure, two different DWTs are executed in parallel in dual-tree structure where the real part of DT-ℂWT is provided by the first one and the imaginary part by the second one.

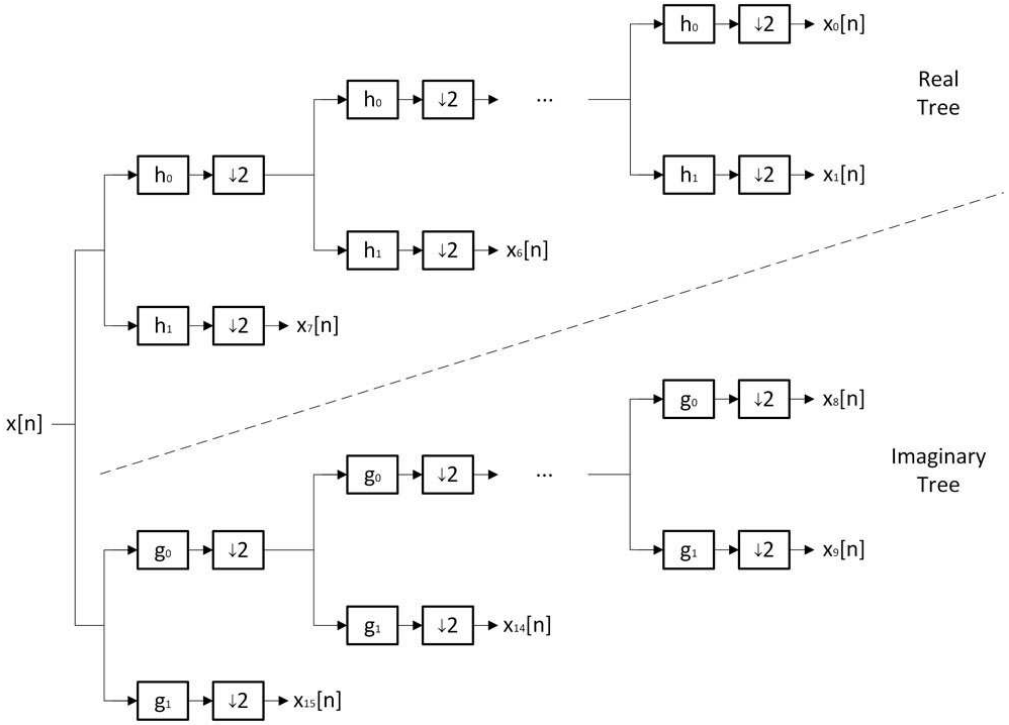

Figure 3.3: Seven-level complex wavelet tree.

Analyticity allows one-dimensional DT-$\mathbb{C}$WT to be approximately shift-invariant and free of aliasing artifacts often encountered in DWT-based processing. Hence, the reasoning behind the use of dual-tree is obtaining an analytic complex wavelet $\psi_c(t)$ through the formula:

$$\psi_c(t) = \psi_h(t) + j\psi_g(t) \tag{3.4}$$

where $\psi_h(t)$ and $\psi_g(t)$ denote wavelet functions of real and imaginary trees, respectively. If $\psi_c(t)$ is approximately analytic (has support on only one-side of the frequency axis), the resulting transform can possess shift-invariance and lack of aliasing properties just like the Fourier transform whose complex basis functions are analytic [61]. For $\psi_c(t)$ to be approximately analytic, it is required that one wavelet basis is the approximate Hilbert transform of the other wavelet basis:

$$\psi_g(t) \approx \mathcal{H}\{\psi_h(t)\} \tag{3.5}$$

Table 3.1: Impulse response of Kingsbury's eighth order q-shift analysis filters for the DT-ℂWT. They are normalized so that $\sum_n h_0[n] = 1$.

Analysis filters	h_0	h_1	g_0	g_1
Q-shift filter coefficients	0.0248	-0.0808	-0.0808	-0.0248
	0	0	0	0
	-0.0624	0.4155	0.4155	0.0624
	0.1653	-0.5376	0.5376	0.1653
	0.5376	0.1653	0.1653	-0.5376
	0.4155	0.0624	-0.0624	0.4155
	0	0	0	0
	-0.0808	-0.0248	0.0248	-0.0808

In order to satisfy the condition in Eq. 3.5, low-pass analysis filters in real and imaginary trees must be offset approximately by half-sample [66]:

$$g_0[n] \approx h_0[n - 0.5] \tag{3.6}$$

In the literature, two low-pass filters are jointly designed such that half-sample delay, perfect reconstruction and finite support conditions are simultaneously satisfied, using several filter design methods [61]. We focused on the q-shift filter design in this thesis and employ them to obtain time-varying lifting filters. Analysis q-shift filters for real and imaginary trees are shown in Table 3.1 [67].

In feature extraction stage, energies of the eight frequency sub-bands of each wavelet tree are used as totally 16 feature parameters. In other words, eight features are obtained from the real part of the complex wavelet and the other eight features are obtained from the imaginary part. As it can be seen from our example, DT-ℂWT suffers from increased data rate in the transform domain. The redundancy factor resulting from DT-ℂWT decomposition of a d-dimensional signal is 2^d [68]. In the next section, the ST-ℂWT method is introduced to prevent this redundancy while providing near shift-invariance and no-aliasing.

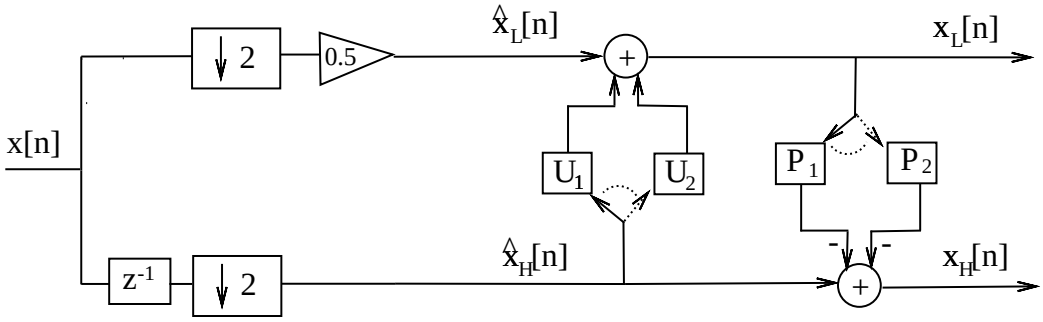

Figure 3.4: Time-varying lifting scheme for the ST-ℂWT.

3.2 Single-Tree Complex Wavelet Transform

We designed real-valued lifting filters to be used in the single-tree context to obtain a transform that is approximately complex in the sense of DT-ℂWT without causing redundancy and a computational burden [69], [70], [71]. The implementation scheme of our real-valued ST-ℂWT design is shown in Figure 3.4.

In Figure 3.4, $U_{1,2}(z)$ and $P_{1,2}(z)$ denote two different sets of update and prediction filters, respectively. Since the aim is to construct an approximately complex wavelet transform using only one tree, the first update filter $U_1(z)$ must correspond to the low-pass analysis filter of the real tree $h_0[n]$ and the second update filter $U_2(z)$ must correspond to the low-pass analysis filter of the imaginary tree $g_0[n]$, of DT-ℂWT, respectively.

Even and odd samples of the sub-signal $x_L[n]$ are obtained using $u_1[n]$ and $u_2[n]$, respectively. Similarly, even and odd samples of $x_H[n]$ are obtained using $p_1[n]$ and $p_2[n]$, respectively. Using u_1 and u_2 in a sequentially switched manner for low-pass filtering of the input signal, we constructed a time-varying single-tree lifting structure that keeps the benefits of DT-ℂWT. More formally, the input signal is first divided into even-indexed samples $\hat{x}_L[n]$ and odd-indexed samples

$\hat{x}_H[n]$ through a lazy filter-bank. Even-indexed samples of $\hat{x}_L[n]$ are updated by $U_1(z)$ and odd-indexed samples of $\hat{x}_L[n]$ are updated by $U_2(z)$. Let $\tilde{h}_1[n]$ and $\tilde{h}_2[n]$ denote the effective half-band low-pass filters processing the input signal $x[n]$ before downsampling. Their z-transforms are given by

$$\tilde{H}_1(z) = 1/2 + z^{-1}U_1(z^2) \tag{3.7}$$

$$\tilde{H}_2(z) = 1/2 + z^{-1}U_2(z^2) \tag{3.8}$$

We designed filters $U_1(z)$ and $U_2(z)$, or equivalently $\tilde{H}_1(z)$ and $\tilde{H}_2(z)$ using the following constraints so that the resulting transform is approximately complex:

(i) Since $\tilde{h}_i[n]$ is a half-band filter, $\tilde{h}_i[2n] = 0$ for $n \neq 0$, $i = 1, 2$, for perfect reconstruction in a lifting structure.

(ii) Filters $\tilde{h}_1[n]$ and $\tilde{h}_2[n]$ must have approximate group delays of 1/4 and 3/4, respectively so that there exist 0.5 delay difference between the two filters [34].

(iii) Filters $\tilde{H}_1(z)$ and $\tilde{H}_2(z)$ must have a zero at $z = -1$, that is, $\sum_n \tilde{h}_i[n](-1)^n = 0$ for $i = 1, 2$ so that $\tilde{H}_i(e^{jw}) = 0$ at $w = \pi$.

Based on the constraint (i) the 7-th order FIR filter should be in the following form:

$$\tilde{h}_1[n] = \{\alpha_1, 0, \alpha_2, \alpha_3, \alpha_4, 0, \alpha_5\} \tag{3.9}$$

where α_3 denotes the coefficient at $n = 0$. We can use the three dominant center coefficients of h_0 from Table 3.1 to obtain α_2, α_3 and α_4 as follows

$$\alpha_2 = 0.1538, \alpha_3 = 0.5, \alpha_4 = 0.3864 \tag{3.10}$$

which are scaled versions of $h_0[3]$, $h_0[4]$, and $h_0[5]$, respectively. Since the filter coefficients in Eq. 3.9 must sum to one, we have

$$\alpha_1 + \alpha_5 = -0.0402 \tag{3.11}$$

To satisfy the constraint (iii), we need

$$\alpha_3 - \sum_{i \neq 3} \alpha_i = 0 \tag{3.12}$$

which is already satisfied by setting $\alpha_3 = 0.5$. The final constraint to satisfy is the half-sample delay the constraint (ii). The group delay of the filter $\tilde{h}_1[n]$ is given by

$$\tau_g(w) = -\frac{\partial \phi(w)}{\partial w} \tag{3.13}$$

where $\phi(w) = arg\{\tilde{H}_1(e^{jw})\}$ is the phase of the DTFT of $\tilde{h}_1[n]$. The frequency response of $\tilde{h}_1[n]$ is given by:

$$\tilde{H}_1(e^{jw}; \alpha_1) = \alpha_1 e^{3jw} + \sum_{i=2}^{4} \alpha_i e^{(3-i)jw} + (-0.0402 - \alpha_1) e^{-3jw} \tag{3.14}$$

where α_1 is the only unknown. The filter coefficient α_1 can be easily determined by one-dimensional exhaustive search in the interval of $[-1, 1]$. First, for each $\alpha \in [-1, 1]$ we fitted a linear model to the phase $\phi(w; \alpha) = arg\{\tilde{H}_1(e^{jw}; \alpha)\}$. The reason is that the q-shift filters are approximately linear phase and have almost constant group delay [67]. Fitting process is performed for the low frequencies ($w \in [-\frac{\pi}{2}, \frac{\pi}{2}]$) because approximately linear behaviour of the phase function disappears as the w approaches to $\pm\pi$. After fitting the linear model, the negative slope of the resultant line yields the group delay of the filter obtained from Eq. 3.13. To have a group delay of 1/4, it turns out that

$$\alpha_1 = -0.05, \alpha_5 = 0.0098 \tag{3.15}$$

The second filter $\tilde{h}_2[n]$ is simply the time reversed version of the filter $\tilde{h}_1[n]$. This is similar to the time reversed design of $\{h_0, g_0\}$ filter pair in [67]. Hence, $\tilde{h}_2[n]$ is given by

$$\tilde{h}_2[n] = \{\alpha_5, 0, \alpha_4, \alpha_3, \alpha_2, 0, \alpha_1\} \tag{3.16}$$

Since $\tilde{h}_2[n]$ is the time-reversed version of $\tilde{h}_1[n]$ they approximately satisfy the half-sample delay condition given in Eq. 3.6. It is possible to implement these two

filters after decimation because they can be expressed in half-band form given in Eq. 3.7 and 3.8 where

$$U_1(z^2) = \alpha_5 z^{-2} + \alpha_4 + \alpha_2 z^2 + \alpha_1 z^4 \tag{3.17}$$

$$U_2(z^2) = \alpha_1 z^{-2} + \alpha_2 + \alpha_4 z^2 + \alpha_5 z^4 \tag{3.18}$$

Prediction filters $P_1(z)$ and $P_2(z)$ are designed by applying the same design strategy as in update filters. In prediction, $P_1(z)$ uses only those samples of the signal $x_L[n]$ which are updated by $U_1(z)$ and $P_2(z)$ uses only those samples of the signal $x_L[n]$ which are updated by $U_2(z)$. From Table 3.1, $h_1[n] = (-1)^n h_0[N-1-n]$ where N is the length of the filter. Thus, effective prediction filter corresponding to $P_1(z)$ is given by

$$\tilde{g}_1[n] = \{-\alpha_5, 0, -\alpha_4, \alpha_3, -\alpha_2, 0, -\alpha_1\} \tag{3.19}$$

Since $g_1[n] = h_1[N-1-n]$ from Table 3.1, effective prediction filter corresponding to $P_2(z)$ is given by

$$\tilde{g}_2[n] = \{-\alpha_1, 0, -\alpha_2, \alpha_3, -\alpha_4, 0, -\alpha_5\} \tag{3.20}$$

Update and prediction filters designed above are employed at the second decomposition level or higher. For the first level, half-sample delay condition in Eq. 3.6 becomes one-sample delay condition for DT-$\mathbb{C}$WT to be approximately analytic at each level [61]. Hence, simple $\{1/2, 1/2\}$ filter is used as the effective update filter at the first level, and the coefficient at $n = 0$ is changed between U_1 and U_2. For prediction at the first level, $\{-1/4, 1, 3/4\}$ effective prediction filter is employed, which assigns weights to the samples based on their proximity to the predicted sample.

For our ST-$\mathbb{C}$WT application, input signals are again fed to a seven-stage wavelet-tree and feature parameters are extracted by finding the energies of resulting eight frequency sub-bands. Frequency boundaries are formed in the same manner with the DWT as described in Section 3.1.

3.3 Shift-Invariance Property Based Comparison

To investigate the shift-invariance property for the aforesaid frequency analysis methods, a unit step signal and its shifted versions are given as input to the wavelet filter-banks, and the wavelet coefficients at the third level are determined. The input signal and, four-sample and five-sample shifted versions are shown in Figure 3.5. The wavelet coefficients of the Haar wavelet, Daubechies-2 wavelet, Daubechies-4 wavelet, Biorthogonal-3.3 wavelet, DT-$\mathbb{C}$WT, and ST-$\mathbb{C}$WT are shown in Figure 3.6, 3.7, 3.8, 3.9, 3.10, and 3.11, respectively. The energies of the wavelet coefficients for the third level decomposition are calculated. Then, change amounts in these energies are observed while shifting the input signal to investigate the shift-invariance properties of the frequency analysis schemes.

Near shift-invariance properties of the DT-$\mathbb{C}$WT and ST-$\mathbb{C}$WT are obvious from the figures. The wavelet coefficients are not much affected by shifts in the input signal for the DT-$\mathbb{C}$WT and ST-$\mathbb{C}$WT whereas DWT-based methods may yield very different output signals as a response to small translations of the input signal. The Haar wavelet is incapable of dealing with one-sample shifted signals and it can be seen from Figure 3.6. The other DWT-based methods also do not provide satisfactory results while shifting the unit step signal four and five samples. For the DT-$\mathbb{C}$WT and ST-$\mathbb{C}$WT methods, input signal and its shifted versions provide very similar results considering the energies of the wavelet coefficients.

Some other experiments are conducted using the vibration sensor signal in Section 4.3.1. In these experiments, the frequency analysis methods are compared to each other in a similar way with the unit step signal example. However, the ST-$\mathbb{C}$WT method should be applied to various applications to see if it really provides near shift-invariance like the DT-$\mathbb{C}$WT.

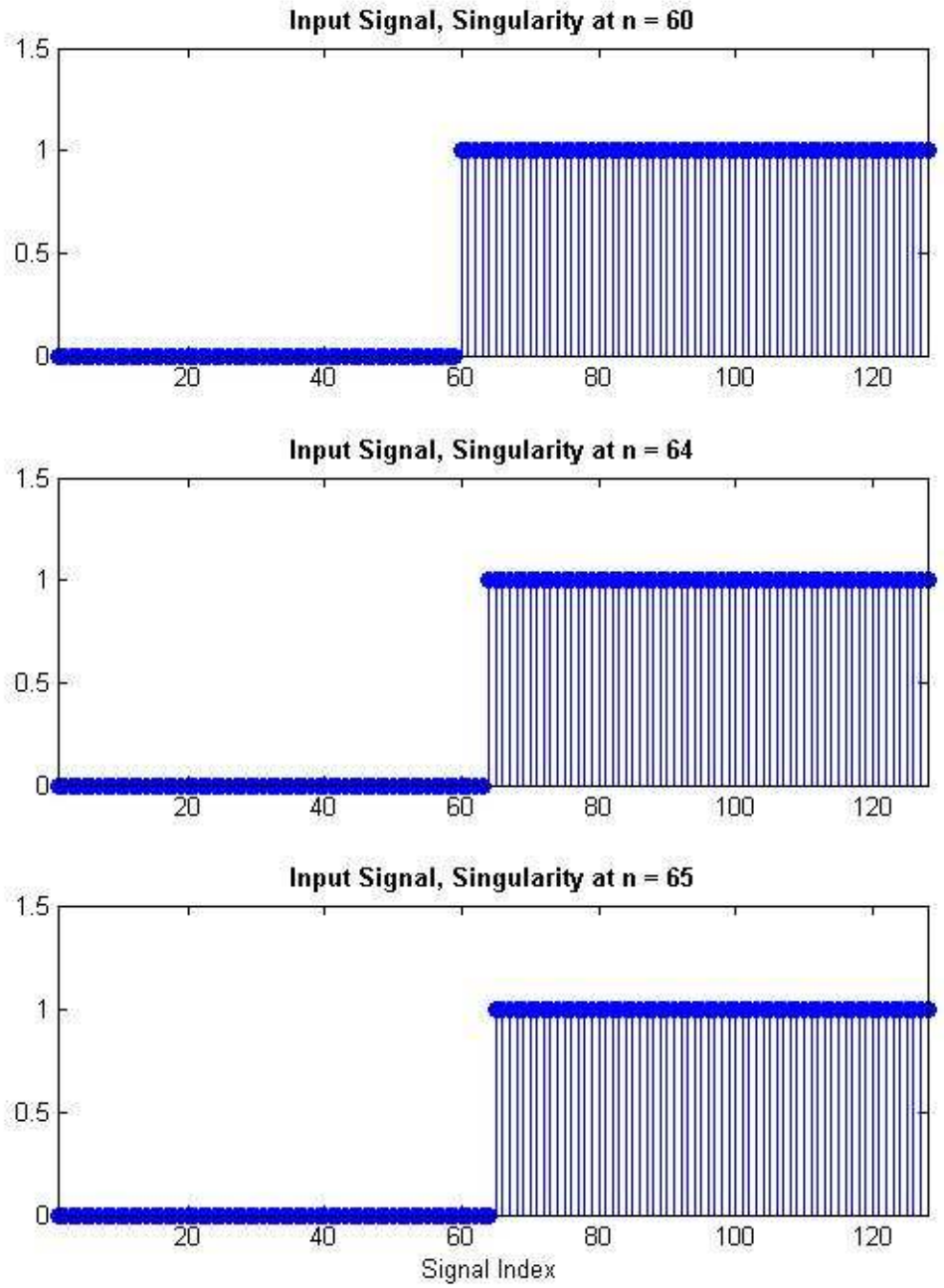

Figure 3.5: A unit step signal, and its four-sample and five-sample shifted versions.

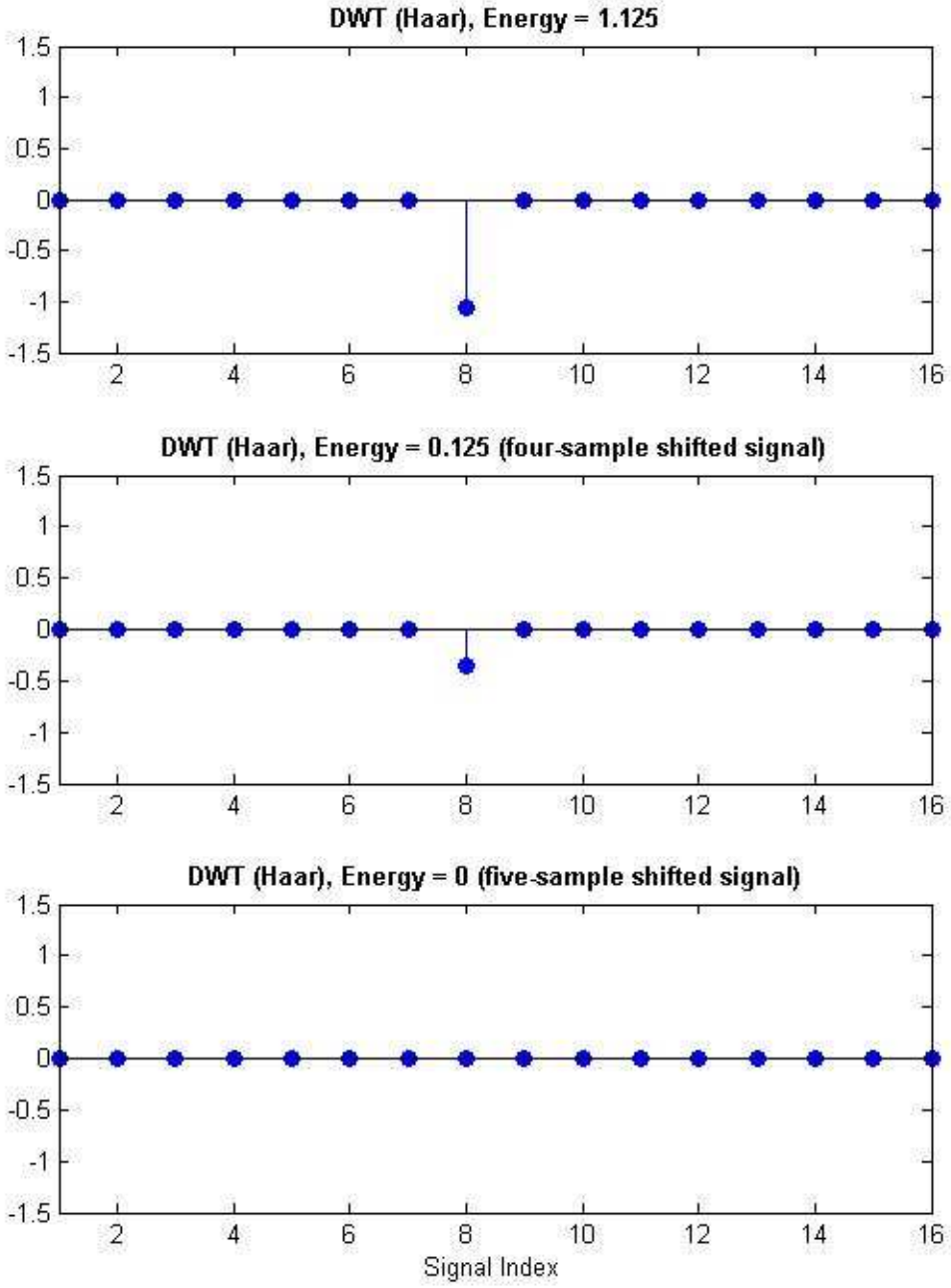

Figure 3.6: Third level wavelet coefficients of a unit step signal and its shifted versions for the Haar wavelet.

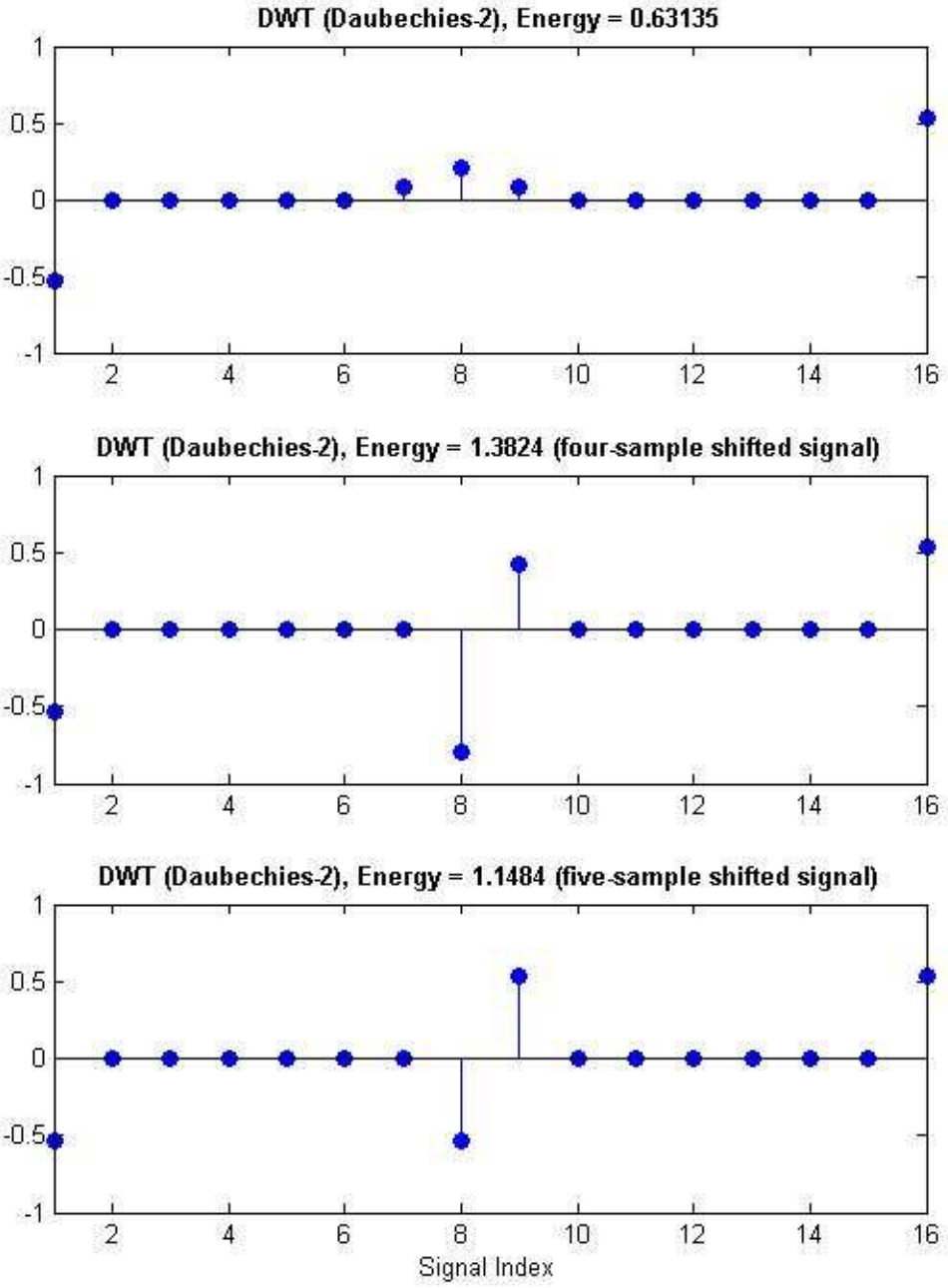

Figure 3.7: Third level wavelet coefficients of a unit step signal and its shifted versions for the Daubechies-2 wavelet.

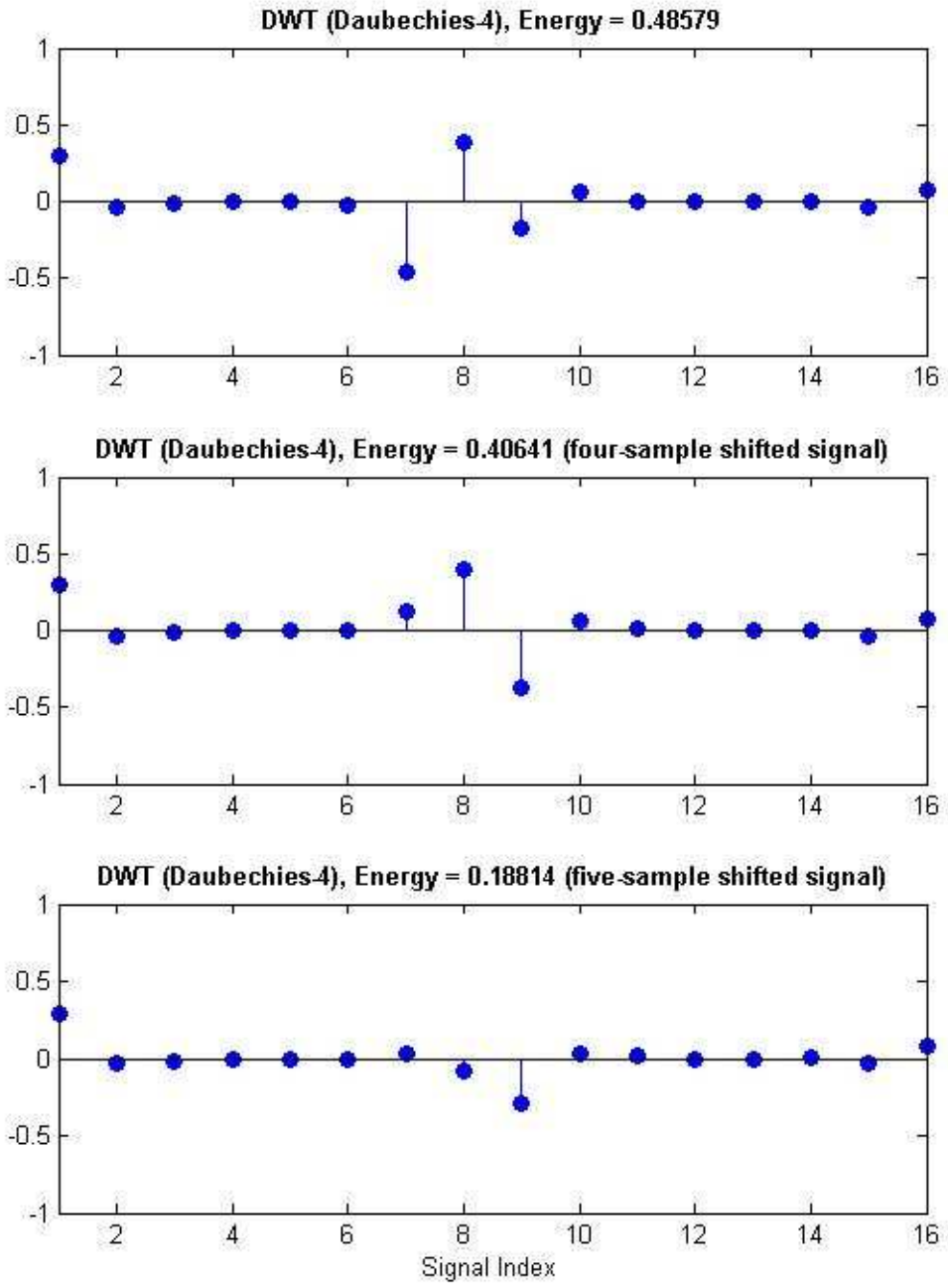

Figure 3.8: Third level wavelet coefficients of a unit step signal and its shifted versions for the Daubechies-4 wavelet.

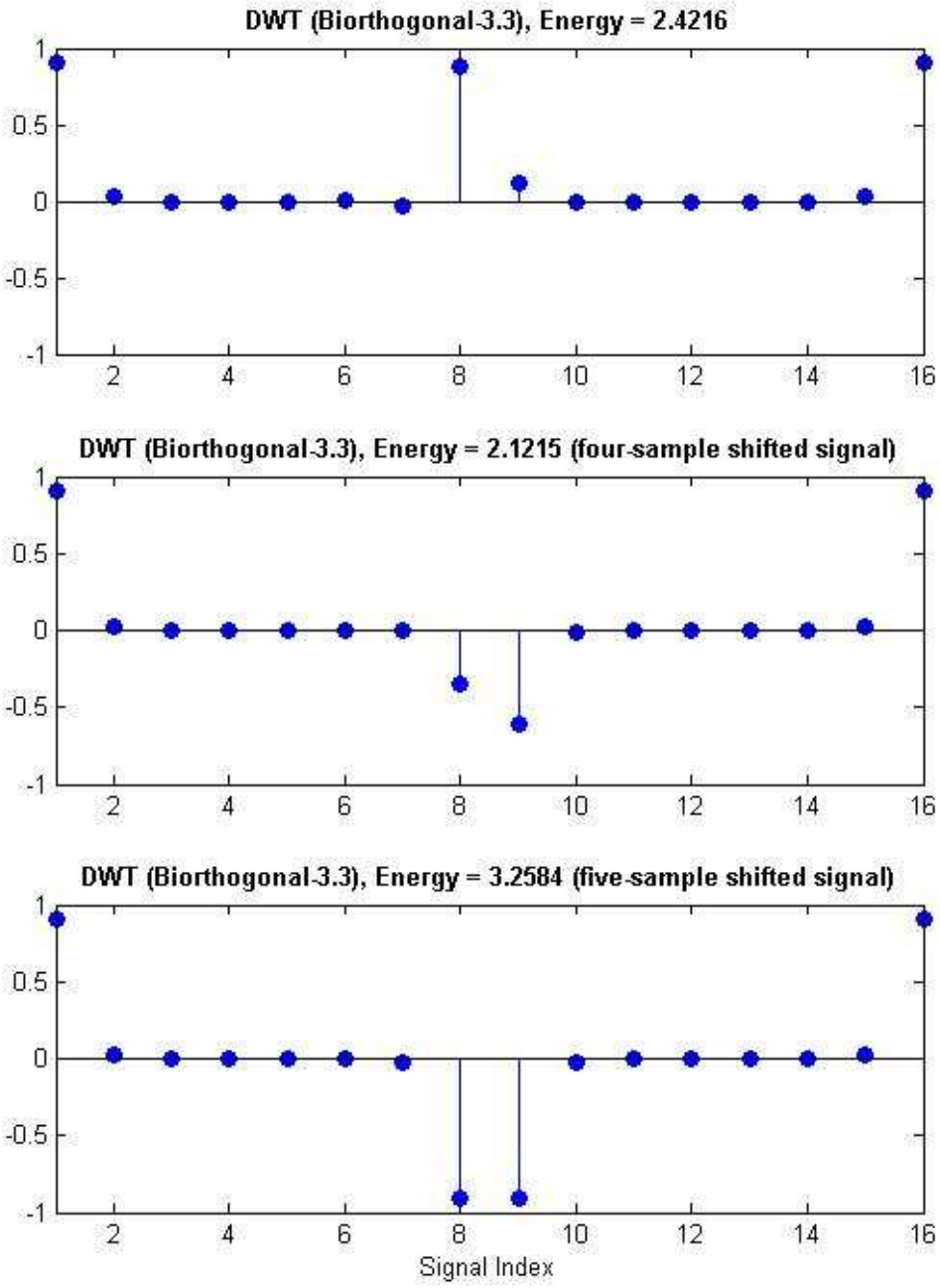

Figure 3.9: Third level wavelet coefficients of a unit step signal and its shifted versions for the Biorthogonal-3.3 wavelet.

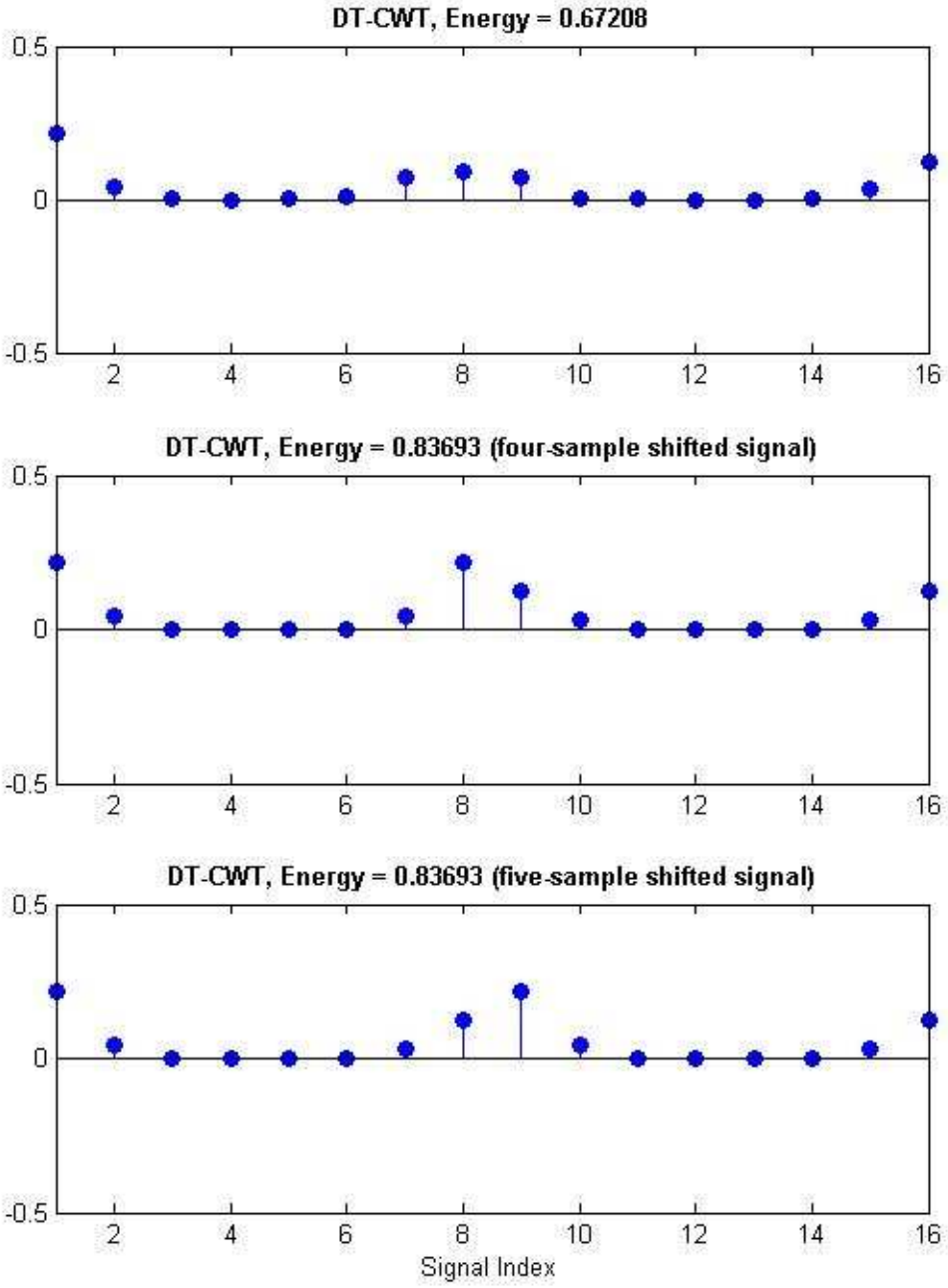

Figure 3.10: Third level wavelet coefficients of a unit step signal and its shifted versions for the DT-ℂWT wavelet.

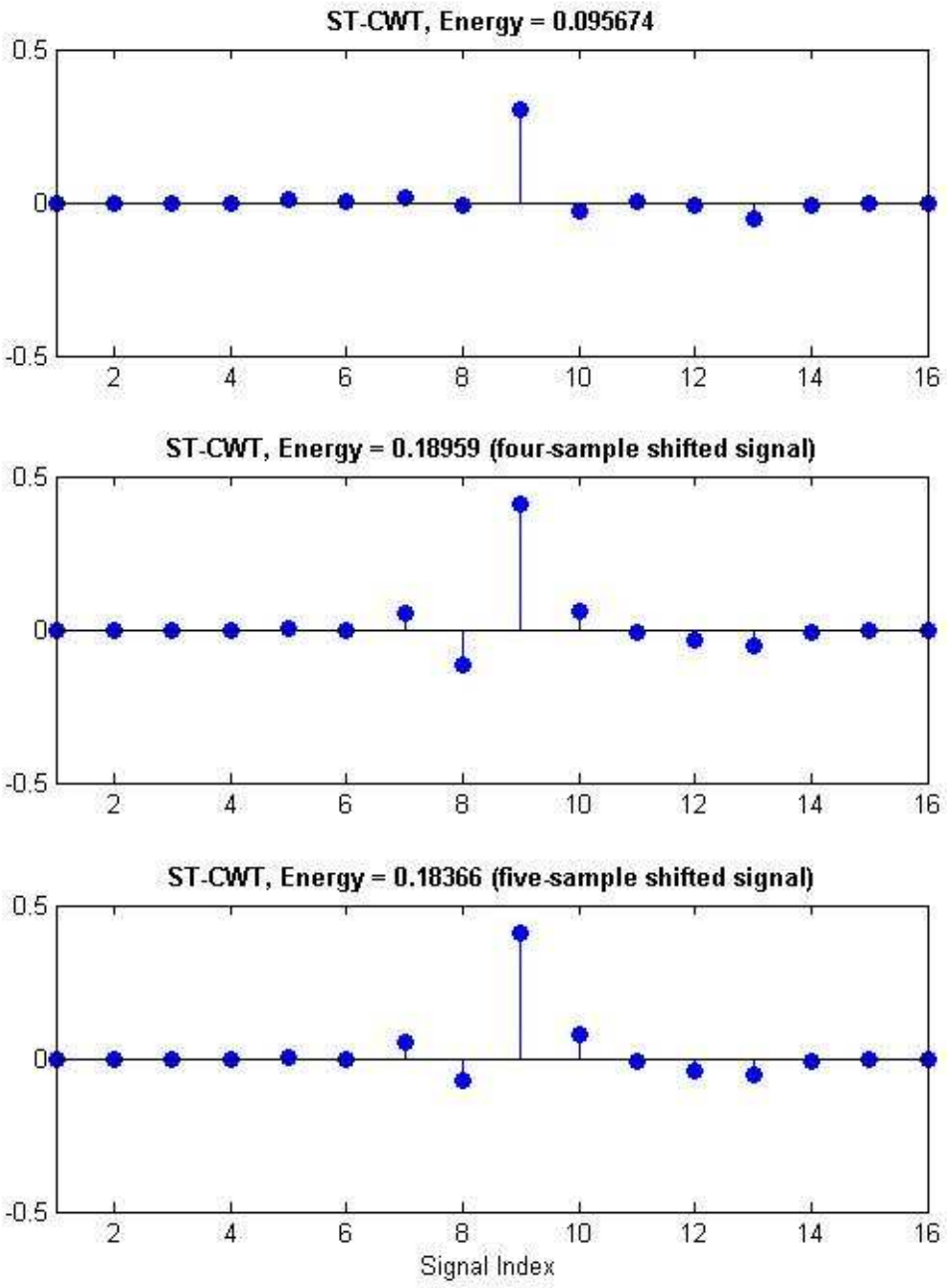

Figure 3.11: Third level wavelet coefficients of a unit step signal and its shifted versions for the ST-ℂWT wavelet.

3.4 Computational Complexity Based Comparison

The DFT, MFCC, DWT, DT-$\mathbb{C}$WT and ST-$\mathbb{C}$WT are compared to each other in terms of computational complexity. For the numerical examples, number of the signal samples over one signal window, N, is taken 1024, and number of the frequency sub-bands, M, is taken 8.

Fast Fourier transform (FFT) is utilized instead of the DFT in the tests. The N-point FFT requires $N \log_2 N$ complex multiplications and additions. Besides, N real multiplications are needed to calculate the energies of the frequency sub-bands. Therefore, computational complexity of the DFT based feature extraction method is on the order of $O(N \log_2 N)$.

The mel-cepstrum based feature extraction scheme needs an extra $M \log_2 M$ real multiplications and additions to carry out the inverse discrete cosine transform, where M is the number of mel-frequency cepstral coefficients and also the number of frequency sub-bands. Therefore, the computational complexity of the MFCC method is $O(N \log_2 N) + O(M \log_2 M)$. If $N >> M$, it can be used as $O(N \log_2 N)$. In addition, M look-up operations are needed because the log operation is performed by a look-up table.

The computational cost of the DT-$\mathbb{C}$WT is twice that of ordinary DWT which can be implemented in $O(N)$, where N is the number of samples in the signal [72]. The computational complexity of the ST-$\mathbb{C}$WT is equivalent to the ordinary DWT. In each branch of wavelet-tree, the computational cost is equivalent to a discrete convolution operation. If it is a r-level wavelet-tree, $2r$ convolutional operations are needed. Also, if the number of nonzero filter coefficients is p, the number of the real multiplications is also p to get one convolutional output. Totally $2pN(1 - 1/2^r)$ real multiplications are required to execute the ST-$\mathbb{C}$WT. In additionally, the energy values of the frequency sub-bands are computed with $N(1 - 1/2^r) + (r + 1)$ real multiplications. The exact number of all real multiplications is given in Table 3.2.

Table 3.2: The exact number of real multiplications in the feature extraction methods we used. $N = 1024$ is the number of signal samples in each window; $M = 8$ is the number of the frequency sub-bands; p is the number of nonzero filter coefficients, and $r = 7$ is the number of the levels in a wavelet-tree.

DFT	$2N \log_2 N + N$	**21504 multiplications**
MFCC	$2N \log_2 N + N + 2M \log_2 M$	**21552 multiplications**
DWT	$2pN(1 - 1/2^r) + N(1 - 1/2^r) + (r + 1)$	$p = 5$**, 11184 multiplications**
DT-$\mathbb{C}$WT	$2[2pN(1-1/2^r)+N(1-1/2^r)+(r+1)]$	$p = 6$**, 26432 multiplications**
ST-$\mathbb{C}$WT	$2pN(1 - 1/2^r) + N(1 - 1/2^r) + (r + 1)$	$p = 5$**, 11184 multiplications**

The ST-$\mathbb{C}$WT is a computationally efficient method in comparison to the DFT, the MFCC, and the DT-$\mathbb{C}$WT based frequency analysis methods due to the fact that the ST-$\mathbb{C}$WT is designed using lifting structures in a single-tree.

3.5 Summary

Different frequency analysis methods including the DFT, MFCC, DWT, DT-$\mathbb{C}$WT and ST-$\mathbb{C}$WT are studied and compared to each other. It is shown that the ST-$\mathbb{C}$WT is a computationally efficient method in comparison to the other signal analysis methods including DT-$\mathbb{C}$WT and it also provides the shift-invariance property like the DT-$\mathbb{C}$WT. DWT-based wavelets are also computationally efficient but they can not provide the shift-invariance property.

Chapter 4

Ambient Assisted Living System Using Different Sensors

In this chapter, an AAL system is described using the components introduced in Chapter 2, and the theoretical methods reviewed in Chapter 3. Various detection algorithms and classifiers are employed to implement the AAL system. Human footstep detection, falling person detection, human motion detection, unusual inactivity detection, indoor flooding detection, uncontrolled flame detection, gas leak detection, and pet movement detection are the current capabilities of our systems. It is assumed that only one person lives in a smart home while developing our detection algorithms because the aim of this study is to improve the quality of life of the elderly and handicapped people living alone.

The vibration sensor is employed in human footstep detection, falling person detection, and indoor flooding detection applications. The PIR sensor is employed in human motion detection, unusual inactivity detection, falling person detection, uncontrolled flame detection, gas leak detection, and pet movement detection applications. Uncontrolled flame detection, gas leak detection, and pet movement detection systems were studied before in [57], [58], [73]. Among the previous works, only the uncontrolled flame detection application is integrated to our AAL system for the time being.

In Section 4.1, datasets related with our detection systems are proposed. Human motion and unusual inactivity detection systems are described in Section 4.2. In the same section, walking intensity of the person in a certain time period is calculated through the human footstep detection system. As the most important implementations in this thesis, various falling person detection systems are introduced in Section 4.3. One falling person detection system is implemented using a vibration sensor, and the other one is implemented using two PIR sensors. There is also a multi-sensor based falling person detection system which employs one vibration sensor and two PIR sensors. As a final application, the indoor flooding detection methods are discussed in Section 4.4.

Stand-alone sensor fusion application is introduced in Section 4.5 and all detection systems are used in this multi-sensor application. chipKIT Uno32 boards are employed for each sensor and the auto-dial alarm system is connected to the main Uno32 board which determines final decisions for the emergency situations. Uno32 boards communicate using Cat 5 cables in our implementation. The other design details are given in Section 4.5.

4.1 Datasets

In the experiments, the GS-20DX vibration sensor signal is sampled at a rate of 500 Hz, and the Paradox 476+ PIR sensor signal is sampled at a rate of 100 Hz. Sensor signal records are taken in different experimental environments to analyze the effects of different environments. Third floor of a new building which has a concrete floor, second floor of a old building which has a hardwood floor, and fourth floor of a new building which has a hardwood floor are used for the experiments while recording the vibration sensor signals.

For the PIR sensor based detection algorithms, 20-hour-long signal record is used to detect the human motion and unusual inactivity situations. This dataset is employed in Section 4.2.1. The vibration sensor based human footstep detection system uses an another dataset which contains a total of 10-minute-long record

consisting of walking and no-activity events. Five-minute-long part of this record is used to train a MM classifier, and the other five-minute-long part of the record is used to test the classifier. This dataset is used in Section 4.2.2.

Falling person detection experiments are performed on two different datasets. The first of these datasets contain only vibration sensor signals. To implement a two-PIR-sensor based falling person detection system, a new dataset becomes necessary because there was not any PIR sensor signal records in the first dataset. The second dataset is formed by recording the vibration and the PIR sensor signals synchronously.

A typical falling event lasts about two seconds. Therefore, the first dataset for the falling person detection system contains 1024-sample-long signals corresponding to the following number of incident records: 126 falling, 3937 walking/running, 2600 sitting, 117 fallen book, and 32 slammed door. Among these incident records; 53 falling, 1617 walking/running, 1295 sitting, 11 fallen book, and 44 slammed door cases are used for training classifiers. The remaining records are used as the test dataset. Falling, walking, running, and sitting records are obtained from 10 different people. These people have different weights and heights.

The second dataset for the falling person detection system is composed of totally one-hour-long record containing activities such as falling, walking, running, sitting, and bending. In this dataset, one minute record contains only one falling event because before and after of the event need to be known for the two-PIR-sensor based falling person detection system. That is to say, the two-PIR-sensor based system does not detect the falling person immediately, the system needs to analyze a period of time. Therefore, the second dataset contains 20 falling events (20 minutes) and 40-minute-long no-falling events.

The final dataset is related with the indoor flooding detection. In this dataset, the vibration sensor signals are recorded while water is flowing from the sink to the floor. During this recording, there is not any human-sourced vibrations on the floor. This dataset contains 47 flooding and 76 no-activity records which are formed in two-second-long signals and taken in the bathroom.

4.2 Human Motion and Unusual Inactivity Detection

Smart homes for the elderly and handicapped people need to be designed to monitor their daily activities. The person may not stand up from his/her bed or may faint on where he/she is sitting. Hence, if there is not any human motion for a while, detection of this situation becomes crucial. The PIR sensor is a suitable device for the motion detection tasks. If there is a human motion in a room, all of the motion activities can be detected using the PIR sensor. Similarly, instant human motions can be detected and if there is not any motion in a certain time period, the system can also sense this unusual inactivity situation.

Instant human motion detection can be done using the PIR sensor but there can not be made a classification between a walking person and a waving person. In other words, the PIR sensor based system only sense a human motion, it can not make a decision about which type of human motion activity is occurred. If the daily walking intensity of the person is measured, it may be helpful information for the smart home application. Therefore, a measurement of the walking intensity of the person in a certain time period is calculated through the human footstep detection system which uses the vibration sensor instead of the PIR sensor.

4.2.1 PIR Sensor Based Detection Algorithms

Human motion detection using the PIR sensor is not a complex task. Various simple algorithms can be used to sense the human motion. In this thesis, variance of the PIR sensor signal window is compared with a threshold value to make a decision about human motion. Threshold value is determined as 25 by analyzing the variances of two-second-long PIR sensor signal windows. The PIR sensor signal is almost free of noise and by using this threshold-based method human motion can be detected in a room with 100% accuracy. Flowchart of the PIR sensor based human motion detection algorithm is presented in Figure 4.1. Also different algorithms may give the similar results for the human motion detection.

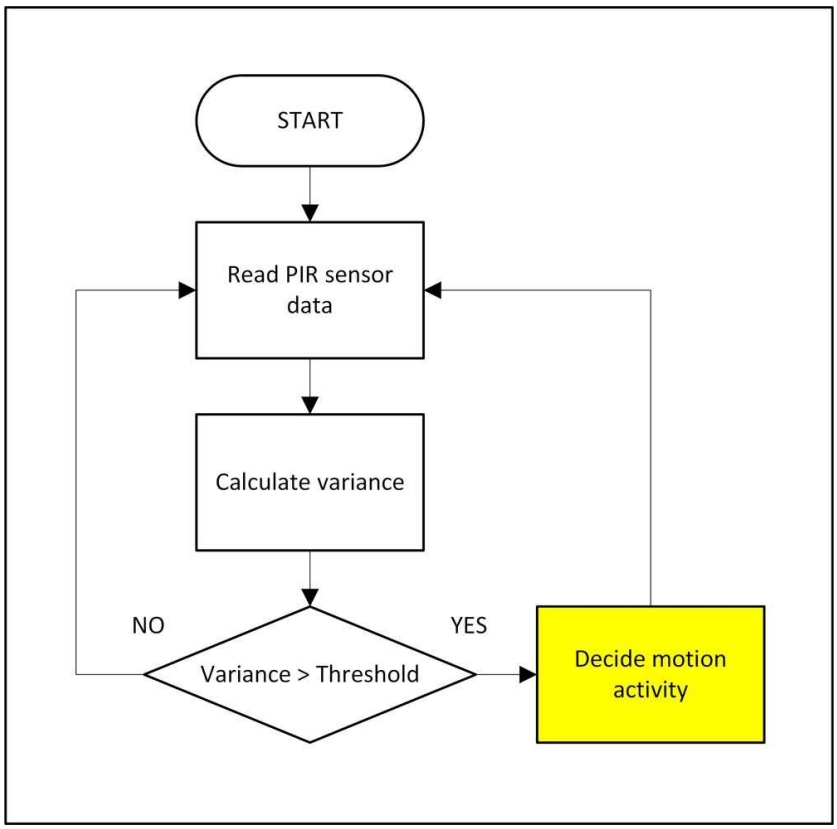

Figure 4.1: Flowchart of the PIR sensor based human motion detection algorithm.

Flowchart of the PIR sensor based unusual inactivity detection algorithm is presented in Figure 4.2. As it can be seen from the flowchart, if there is not any human motion for a while, the person is warned by an alarm to prevent the possible false alarms. The time period is taken 10 minutes to decide the unusual inactivity situation in the tests. If there is no human motion during one minute after the alarm, the system decides that there is an unusual inactivity case and informs the emergency units immediately. Even a small movement is considered as a human motion so the unusual inactivity detection system's accuracy rates are very high. 20-hour-long unusual inactivity record is divided into 10-minute-long segments and a total of 120 segments are tested using the threshold value as 25 for the variance comparison. 100% of the 120 segments are classified correctly.

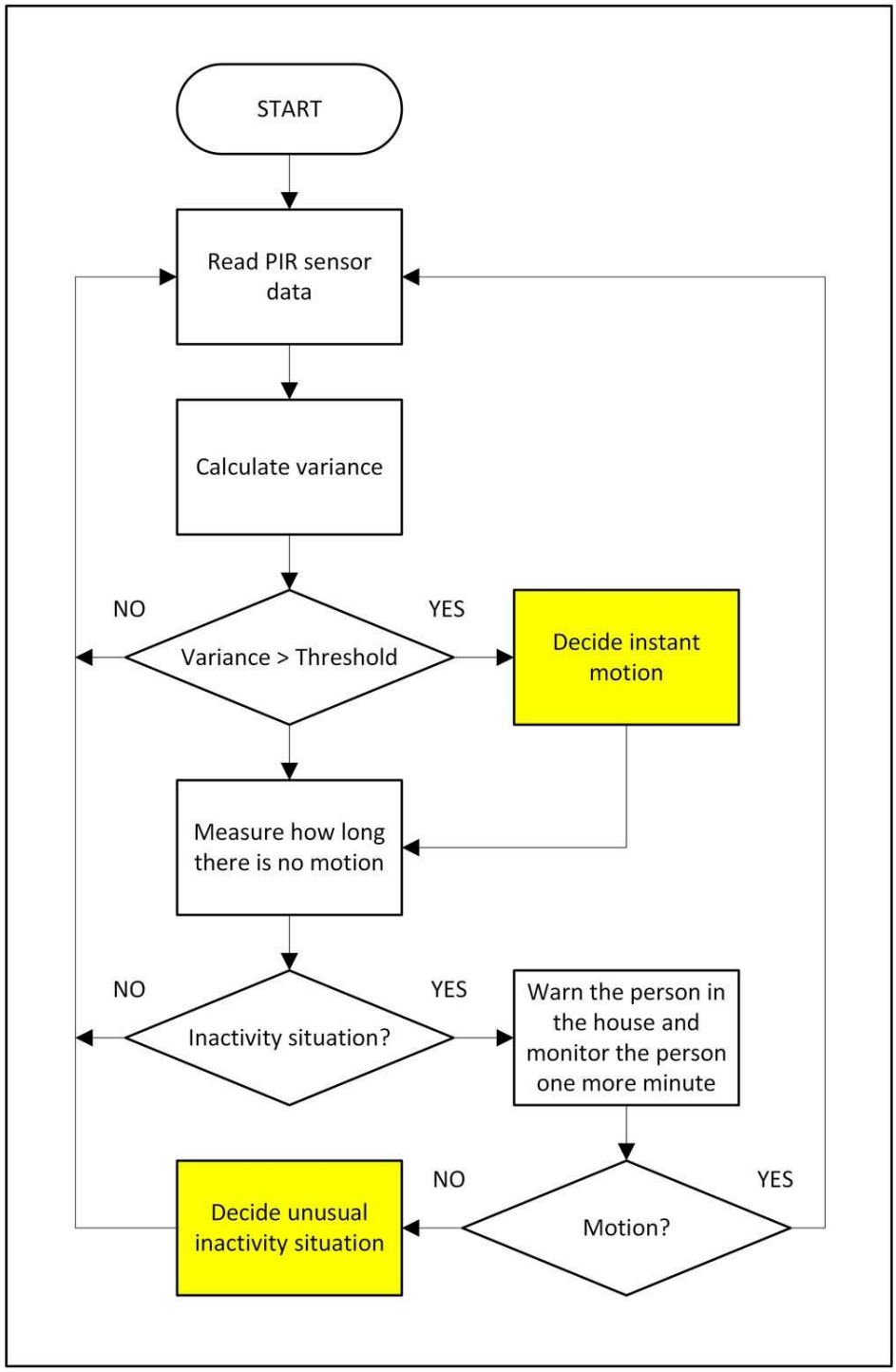

Figure 4.2: Flowchart of the PIR sensor based unusual inactivity detection algorithm.

4.2.2 Vibration Sensor Based Human Footstep Detection

In this subsection, a measurement of the walking intensity of the person in a certain time period is calculated through the vibration sensor based human footstep detection system. Classification between the human-footstep sourced signals and the other signals is done by a MM based system. The MM classifier is trained using the dataset containing five-minute-long record consisting of walking and no-activity events. This dataset is recorded continuously without a pause so that the MM based approach becomes more meaningful.

For the MM classifier one adaptive threshold, T_a, is used and three-state models are trained for each of the classes. To classify a two-second-long vibration sensor signal, x, states are determined by examining the following threshold intervals: $-T_a < x[n] < T_a$ (State-0), $x[n] > T_a$ (State-1), and $x[n] < -T_a$ (State-2). Transitions between these three states are counted for each signal sample and transition matrices are calculated for each two classes of data which consist of walking and no-activity events, respectively. Classification for the testing dataset is done by using the calculated transition matrices. For the human-footstep sourced signals transitions between the three states occur frequently but for the other signals the MM stays at the initial state State-0 mostly. With this observation, the vibration sensor signals are classified into two classes using two different MMs. Mean values of the transition matrices for the training dataset are given in Table 4.1 and 4.2 while T_a is initially set to 4.

Table 4.1: Transition matrix for the human-footstep sourced signals.

	State-0	State-1	State-2
State-0	0.6319	0.0236	0.0305
State-1	0.0236	0.1151	0.0027
State-2	0.0305	0.0027	0.1393

Table 4.2: Transition matrix for the other signal sources.

	State-0	State-1	State-2
State-0	0.9930	0.0009	0.0020
State-1	0.0009	0.0002	0.0000
State-2	0.0020	0.0000	0.0011

However, classification of the vibration sensor signals is not an easy task because the vibration sensor receives almost every vibration in its range like an antenna. Therefore, extracting meaningful information from the sensor signal is critical to make a classification between the signal windows. Signals acquired by vibration sensor may contain various frequency components depending on the architecture of the building in which intelligent home is located. Moreover, running machines in the building may cause additional signal activities. Note also that, amplitudes of vibration signals differ, because they depend on the distance of the person to the sensor and on the pushing-off strength of the foot. Walking very close to the sensor and/or stomping may result in high-amplitude vibration signals. Hence, to handle these kinds of situations adaptive systems are needed.

Algorithm flowchart of the human footstep detection system is presented in Figure 4.3. As it can be seen from the algorithm flowchart, T_a is updated adaptively over time instead of a constant threshold if there is not any human footstep activity in the range of vibration sensor. Variation in the sensor signal originated from the external factors are observed by changing the background variance using the following formula:

$$\sigma_{k,b}^2 = \begin{cases} \sigma_{k-1,b}^2 & \text{if } \sigma_k^2 > \beta\sigma_{k-1,b}^2 \\ \alpha\sigma_{k-1,b}^2 + (1-\alpha)\sigma_k^2 & \text{else} \end{cases} \tag{4.1}$$

where σ_k^2 is the variance of the current signal window and $\sigma_{k,b}^2$ is the background variance. In the experiments, α and β are selected as 0.8 and 1.2, respectively. After that, the adaptive threshold value T_a is updated using the following equation:

$$T_a = T_a \frac{\sigma_{k,b}^2}{\sigma_{k-1,b}^2} \tag{4.2}$$

The aim of using Eq. 4.1 and 4.2 is to eliminate undesired effect of the external factors which include architecture of the building, running machines in the building, etc. If a constant threshold is used instead of an adaptive one, the human footstep detection system may give false alarms while environmental effects are changing. It is also important that adaptive threshold should not be updated when there is a walking person in the environment.

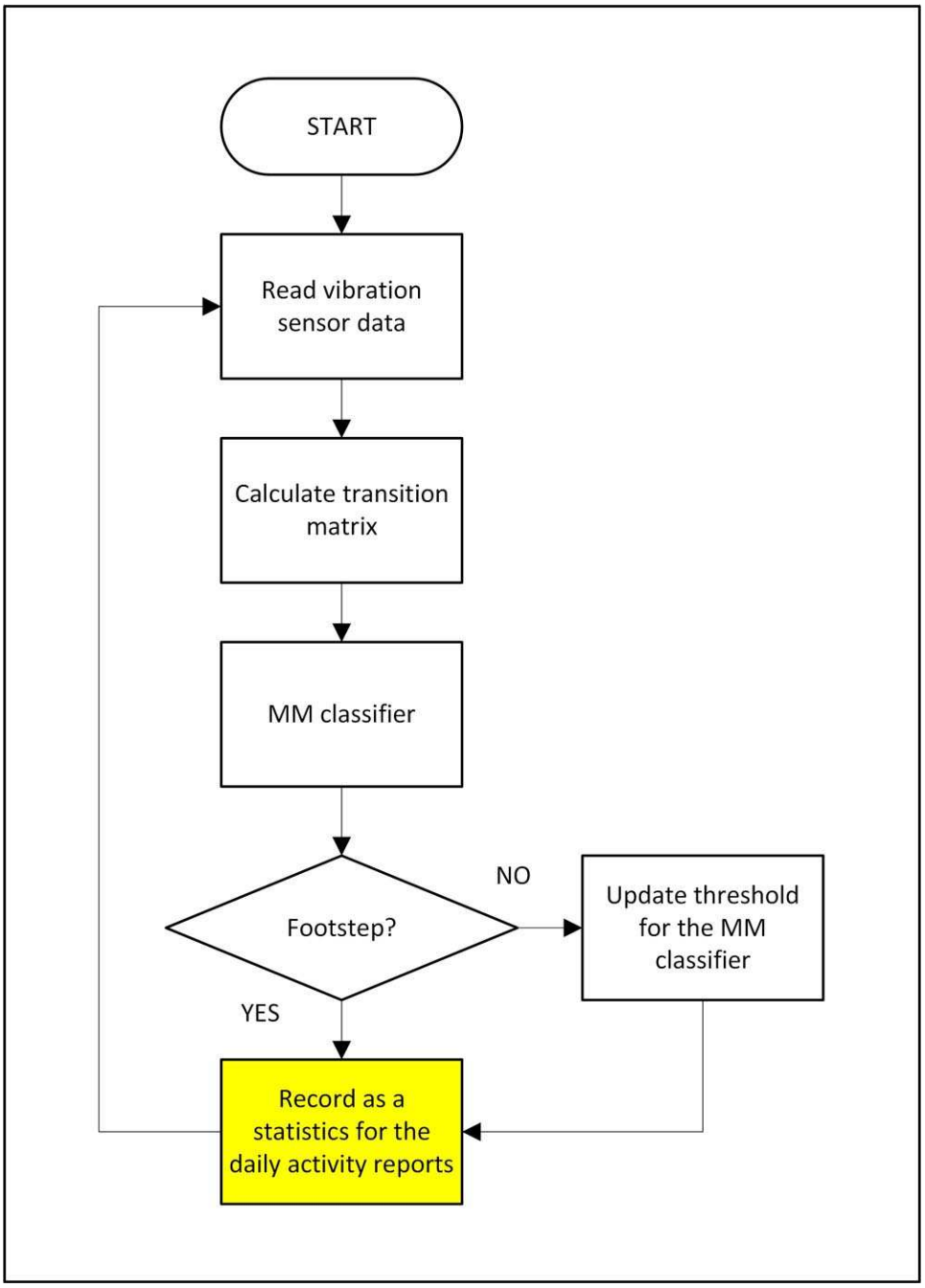

Figure 4.3: Flowchart of the vibration sensor based human footstep detection algorithm.

Table 4.3: Confusion matrix for the human footstep detection system using testing dataset.

Actual Class	Predicted Class	
	Other Sources	**Human Footstep**
Other Sources	109	4
Human Footstep	0	37

Table 4.4: Confusion matrix for the human footstep detection system using all dataset.

Actual Class	Predicted Class	
	Other Sources	**Human Footstep**
Other Sources	199	4
Human Footstep	0	97

After the training of the adaptive-threshold based MM, transition matrices for each of the classes are employed to classify the testing dataset which contains two classes of data. Human-footstep sourced two-second-long signal windows are classified with 100% accuracy and the other signal sources are classified with 96.46% accuracy for the testing dataset. As an other experiment, the all dataset is tested and classification of the other signal sources is made with 98.03% accuracy in this case while human-footstep sourced signal windows are classified with 100% accuracy again. Confusion matrices for these two cases are presented in Table 4.3 and 4.4, respectively.

Training and testing algorithms are developed in MATLAB. After the development of the algorithms, stand-alone system is implemented using chipKIT Uno32 board and integrated to the overall AAL system project. Details of the stand-alone system is given in Section 4.5.

4.3 Falling Person Detection

In this section, various falling person detection applications are introduced. Firstly, a vibration sensor based falling person detection system was developed in our studies [69], [74]. This system uses the theoretical works introduced in Chapter 3 and classifiers which consist of the Euclidean distance and the support vector machine (SVM) classifiers. The experimental setup and statistical results are presented in Section 4.3.1. The vibration sensor based falling person detection system succeeds for many falling situations however it is observed that this system may not detect slow fallings which do not cause a sufficient vibration on the floor. Zero miss-detection rate is crucial for the falling person detection systems and the slow fallings increases miss-detection rates. Hence, a different type of a system is needed to prevent these miss-detections.

In our second system, two PIR sensors are employed concurrently and a novel algorithm is developed to detect a falling person [75]. Details of the two-PIR-sensor based falling person detection system is described in Section 4.3.2. By using this system, the falling event can be analyzed before and after the falling. Therefore, slow fallings also can be detected and the system does not affected by the person or the environment thanks to the PIR sensors. As emphasized before, decreasing the number of false alarms is important but zero miss-detection rate is more important in the falling person detection applications. The two-PIR-sensor based system decreases miss-detection rates as expected.

As a third and last detection system for the falling event, the vibration sensor and two PIR sensors are employed together. This multi-sensor based falling person detection system take advantages of both the vibration sensor based detector and the two-PIR-sensor based detector. For an example, vibration sensor based system can not sense the activities after falling (e.g. standing up) but the two-PIR-sensor based system can analyze the human motions before and after the falling. However, if a person falls fast and stays motionless, the two-PIR-sensor based system finds no way out. In this situations, falling event can be detected instantly using the vibration sensor based system. The other details of the multi-sensor based falling person detection system is presented in Section 4.3.3.

4.3.1 Vibration Sensor Based Detection Algorithm

A typical falling event lasts about two seconds and frequency content of the two-second-long vibration sensor signal window contains useful informations for the classification purposes. Falling person detection system based only on the signal strength may produce false alarms because other signal sources like a falling object situation or a slamming door situation can cause similar vibrations on the floor. To prevent these possible false alarms, duration of the activity and frequency content of the signal window should be taken into account as well as the signal strength.

Our system checks the strength of the vibration sensor signal before analyzing the frequency content of the sensor signal. Signal windows with high deviations from the average value are chosen as candidate fall regions. An experimentally determined value of 50 is used as the threshold. Let $M = \max|x(n)|$ and $m = \min|x(n)|$ within an analysis window of length 1024 samples. When the difference M-m is larger than the threshold, this window of data is further processed by various feature extraction schemes for the falling person detection. If M-m does not exceed the threshold, the human footstep detection system is employed. Flowchart of the vibration sensor based falling person detection algorithm is presented in Figure 4.4.

Candidate fall regions are examined through various frequency analysis methods described in Chapter 3. The DFT, MFCC, DWT with different filter-banks, DT-$\mathbb{C}$WT and ST-$\mathbb{C}$WT are employed to extract features from the 1024-sample-long vibration sensor signals. After the feature extraction, classification for the vibration sensor signals is done between "falling" and "other activities". For this purpose, the Euclidean distance classifier and the SVM classifier are used and compared to each other for the first falling-related dataset introduced in Section 4.1. Comparative results on the detection performance for the feature extraction methods are presented in Table 4.5 and 4.6 according to the Euclidean distance and SVM classifiers, respectively. The results are obtained using the records in the testing dataset.

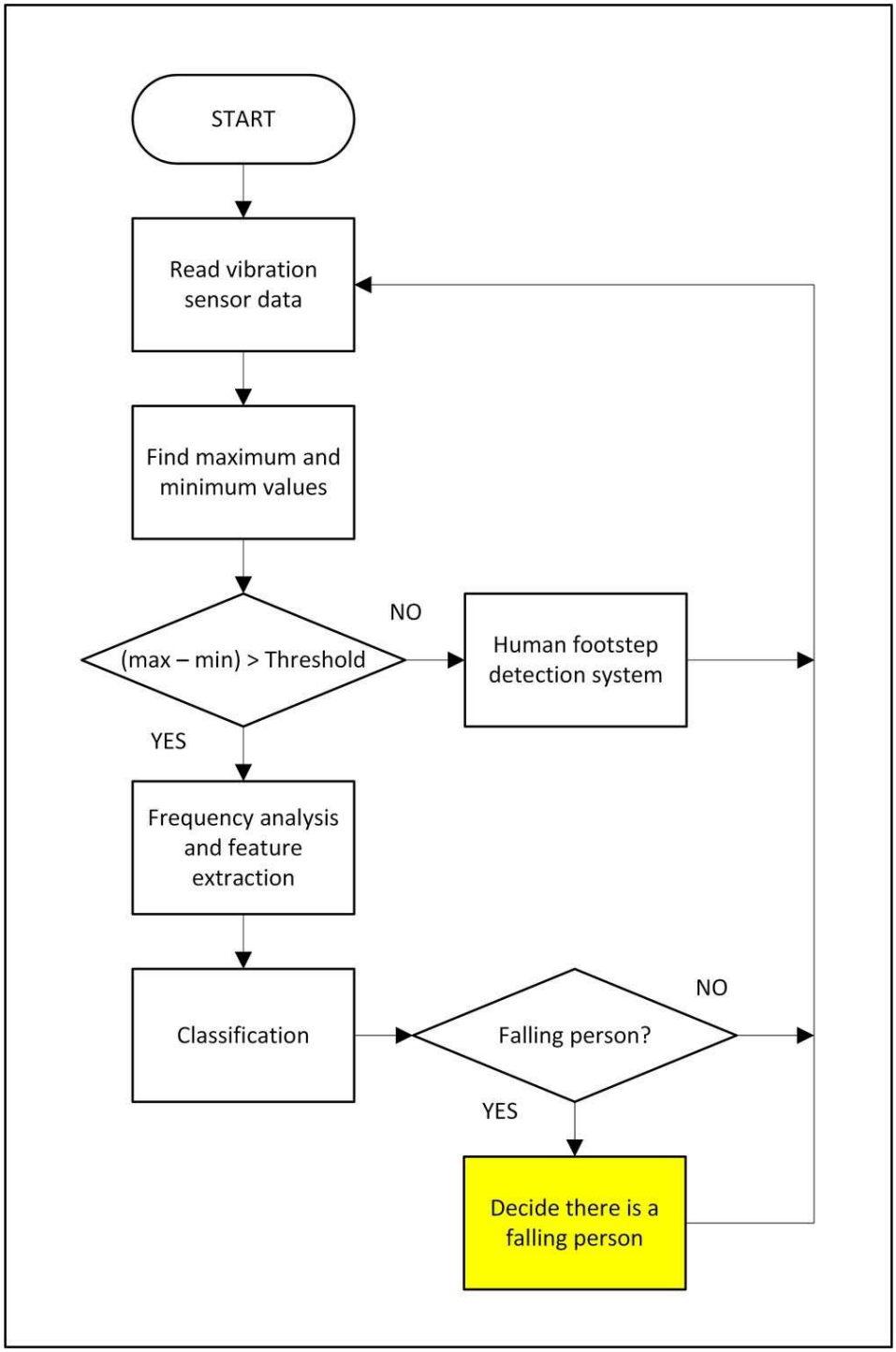

Figure 4.4: Flowchart of the vibration sensor based falling person detection algorithm.

Table 4.5: Numbers of "true detection" versus "false alarm" for 1024-sample-long windows, using the Euclidean distance classifier.

Feature extraction methods	**Falling**	Ordinary activities		Other signal sources	
		Walking/ running	**Sitting**	**Slammed door**	**Fallen book**
Threshold-based	73 / 0	2240 / 80	48 / 9	19 / 2	62 / 11
DFT	60 / 13	2319 / 1	57 / 0	19 / 2	73 / 0
MFCC	63 / 10	2168 / 152	55 / 2	13 / 8	56 / 17
DWT (Haar)	65 / 8	2319 / 1	57 / 0	21 / 0	73 / 0
DWT (Daubechies-2)	63 / 10	2320 / 0	57 / 0	21 / 0	73 / 0
DWT (Daubechies-4)	63 / 10	2320 / 0	57 / 0	21 / 0	73 / 0
DWT (Biorthogonal-3.3)	68 / 5	2320 / 0	57 / 0	21 / 0	73 / 0
DT-$\mathbb{C}$WT	60 / 13	2097 / 223	57 / 0	21 / 0	72 / 1
ST-$\mathbb{C}$WT	60 / 13	2097 / 223	57 / 0	21 / 0	72 / 1

Table 4.6: Numbers of "true detection" versus "false alarm" for 1024-sample-long windows, using the SVM classifier.

Feature extraction methods	**Falling**	Ordinary activities		Other signal sources	
		Walking/ running	**Sitting**	**Slammed door**	**Fallen book**
Threshold-based	73 / 0	2240 / 80	48 / 9	19 / 2	62 / 11
DFT	60 / 13	2320 / 0	57 / 0	19 / 2	73 / 0
MFCC	66 / 7	2259 / 61	57 / 0	21 / 0	69 / 4
DWT (Haar)	70 / 3	2318 / 2	57 / 0	21 / 0	73 / 0
DWT (Daubechies-2)	71 / 2	2315 / 5	57 / 0	21 / 0	73 / 0
DWT (Daubechies-4)	68 / 5	2318 / 2	57 / 0	21 / 0	73 / 0
DWT (Biorthogonal-3.3)	73 / 0	2315 / 15	57 / 0	21 / 0	72 / 1
DT-$\mathbb{C}$WT	71 / 2	2313 / 7	57 / 0	21 / 0	73 / 0
ST-$\mathbb{C}$WT	72 / 1	2316 / 4	57 / 0	21 / 0	72 / 1

There are two classes of data in the dataset: “falling” and “other activities”. In the training stage of the classifiers walking, running, sitting, fallen book, and slammed door records are used all together under the “other activities” class. Then, in the testing stage, classifier models are employed separately for the walking, running, sitting, fallen book, and slammed door records against the “falling” class. The dataset used for the Table 4.5 and 4.6 does not has any experimental results for slow fallings because meanwhile records are taken for this dataset, it is not realized that slow fallings may not be detected by the vibration sensor based system.

Different classifier models are formed for each of the classifiers using the DFT, MFCC, DWT with different filter-banks, DT-$\mathbb{C}$WT and ST-$\mathbb{C}$WT methods and the dataset is tested for each model. It is experimentally observed that the SVM classifier provides better results however the Euclidean distance classifier provides very close results in some of the experiments. The LIBSVM libraries are used for training and testing linear kernel based SVM classifier [76]. It is experimentally observed that the linear kernel based SVM classifier is sufficient to classify the vibration signals as “falling” or “other activity” instead of the more complex kernels like the polynomial and radial basis.

Experimental results indicate that falling, walking, running, sitting, slammed door, and fallen book cases are classified into “falling” and “other activities” classes with high accuracy rates using the wavelet-based frequency analysis methods with the SVM classifier. The DFT and the MFCC based features do not provide satisfactory results in our dataset. A threshold-based classifier falls behind in the results, as expected. By the way, all vibration sensor signal windows in the dataset are shifted with a certain number of the samples to show the shift-invariance properties of the DT-$\mathbb{C}$WT and the ST-$\mathbb{C}$WT. In Table 4.7 and 4.8, numbers of the different classifications between the original signals and 64-sample shifted version of the original signals for 1024-sample-long vibration sensor signal windows are presented for the Euclidean distance and SVM classifiers, respectively. The same classifier models are employed and training processes do not performed again.

Table 4.7: Numbers of the different classifications between the original signals and 64-sample shifted version of the original signals for 1024-sample-long vibration sensor signal windows, using the Euclidean distance classifier.

Feature extraction methods		Ordinary activities		Other signal sources	
	Falling	**Walking/ running**	**Sitting**	**Slammed door**	**Fallen book**
DFT	0	0	0	0	0
MFCC	5	3	0	1	1
DWT (Haar)	2	1	0	0	0
DWT (Daubechies-2)	0	0	0	0	0
DWT (Daubechies-4)	0	0	0	0	0
DWT (Biorthogonal-3.3)	5	250	0	0	3
DT-$\mathbb{C}$WT	0	0	0	0	0
ST-$\mathbb{C}$WT	0	0	0	0	0

Table 4.8: Numbers of the different classifications between the original signals and 64-sample shifted version of the original signals for 1024-sample-long vibration sensor signal windows, using the SVM classifier.

Feature extraction methods		Ordinary activities		Other signal sources	
	Falling	**Walking/ running**	**Sitting**	**Slammed door**	**Fallen book**
DFT	0	2	0	0	0
MFCC	1	3	0	0	1
DWT (Haar)	2	1	0	0	0
DWT (Daubechies-2)	2	3	0	0	0
DWT (Daubechies-4)	0	0	0	0	0
DWT (Biorthogonal-3.3)	0	91	7	0	16
DT-$\mathbb{C}$WT	0	0	0	0	0
ST-$\mathbb{C}$WT	0	0	0	0	0

Table 4.9: Change amounts in the energy of the fourth level wavelet coefficients or the corresponding frequency sub-band while shifting the 1024-sample-long vibration sensor signal windows. Lower numbers mean that shift-invariance is provided better by the related frequency analysis methods. Experiment is repeated for 1000 different signal windows and average values are given.

	10-sample shifting	**15-sample shifting**	**25-sample shifting**	**50-sample shifting**
DWT (Haar)	17.97%	11.96%	15.73%	16.34%
DWT (Daubechies-2)	15.44%	9.37%	12.72%	13.59%
DWT (Daubechies-4)	12.48%	6.09%	10.49%	10.37%
DWT (Biorthogonal-3.3)	20.99%	15.13%	15.99%	21.22%
DT-ℂWT	0.56%	0.53%	0.41%	0.52%
ST-ℂWT	4.32%	4.48%	4.57%	4.34%

Table 4.7 and 4.8 are formed using the classification results of the original signal windows and the shifted signal windows. If the classification results are different, each different signal window is counted to see how the results differ when the signal windows are shifted. The classification results for the Daubechies-4 wavelet, the DT-ℂWT, and the ST-ℂWT do not change while shifting the original signal windows. However, the Biorthogonal-3.3 wavelet does not provide satisfactory results in the same case. Actually, the shift-invariance property may not be tested accurately in this experimental setup because the energies of the frequency subbands are used as feature parameters and the fine details of the frequency content does not effect the final classification result. Therefore, an another experiment is conducted. In this experiment, change amounts in the energy of the fourth level wavelet coefficients or the corresponding frequency sub-band while shifting the 1024-sample-long vibration sensor signals are analyzed as presented in Table 4.9. Different numbers of shifting are tested and it is observed that the DT-ℂWT and the ST-ℂWT based decompositions provide a better shift-invariance property in comparison to the other wavelet-based methods. In Table 4.9, average values of the 1000 signal windows are given.

Table 4.10: Confusion matrix for the vibration sensor based falling person detection system using the second dataset. This dataset is composed of one-minute-long records which correspond to the one sample for every one minute.

Actual Class	Predicted Class	
	Other Sources	**Falling Person**
Other Sources	36	4
Falling Person	7	13

The vibration sensor based detection of a falling person instantly has some advantages and disadvantages. A remarkable advantage of these system is that the first-aid to the falling person may be done without wasting time. However, as an important disadvantage, the vibration sensor based systems may not detect slow fallings which do not cause a sufficient vibration on the floor and miss-detection rates increase in this way. The dataset used for Table 4.5 and 4.6 does not has any slow fallings. Hence, to analyze the classification of the slow falling event, the second dataset is employed. In this second dataset, there are also signal records for the two-PIR-sensor based system.

The second dataset is composed of one-minute-long records containing activities such as falling, walking, running, sitting, and bending. For the falling-related part of this dataset, one-minute-long record contains one falling event and the falling can happen at any time in this one minute. Some of the falling events are soft fallings and some of them are not. In Table 4.10, experimental results of the second dataset are presented. Threshold-based classifier is preferred in this time because there are not enough signal records to train a classifier model. Considering the results, false alarms are caused by sitting on the floor instantly because in this situation, energy of the vibration signals increase like a falling person case. Additionally, soft fallings cause miss-detections as shown in Table 4.10.

The second dataset is also employed in Section 4.3.2 and 4.3.3 to compare different detection systems while realizing the superiorities of these systems.

4.3.2 Two-PIR-Sensor Based Detection Algorithm

The PIR sensor signal by itself does not contain too much information. For an example, a walking person may be the cause of a signal as a falling person causes. However, two or more PIR sensors can enrich the information obtained for different purposes. In this sub-section, two PIR sensors are employed to detect falling person in different manner from the previous falling person application described in Section 4.3.1.

In our system, two PIR sensors are employed concurrently and a novel algorithm is developed to detect a falling person. This algorithm uses information of the human motion activities in different heights. Positions of two PIR sensors are adjusted to see upper and lower parts of a walking person separately. As emphasized in Section 2.3.1, lens structure of the PIR sensor is designed to cover the lower section of the horizontal level of the sensor as previously presented in Figure 2.8. In our design, the lower PIR sensor is aligned with the knees and the upper PIR sensor which is turned upside down is aligned with the waist as illustrated in Figure 4.5. If the lower PIR sensor detects some human motion activities and the upper PIR sensor does not detect any human motion activities for a while, the system decides that it can be falling person in the related room. An example falling person case is illustrated in Figure 4.6.

The flowchart of the two-PIR-sensor based falling person detection algorithm is presented in Figure 4.7. One-second-long signal windows are analyzed to detect a human motion in every second. Threshold value 10 is used for the human motion detection through the variance-based algorithm described in Section 4.2.1. The motion detection results are stored separately for the last one minute. Eventually, there are two 60-element result vectors which store human motion activities of last one minute as a logic zero or logic one. If the motion activity of lower PIR sensor is higher than the motion activity of upper PIR sensor and if there are too few human motion activities in the range of upper sensor for the last one minute, it means there may be a falling person in the room. We preferred to analyze last one minute records however different lengths also can be selected. Certainly, if five minutes is selected toward the past, the necessary first-aid may be late.

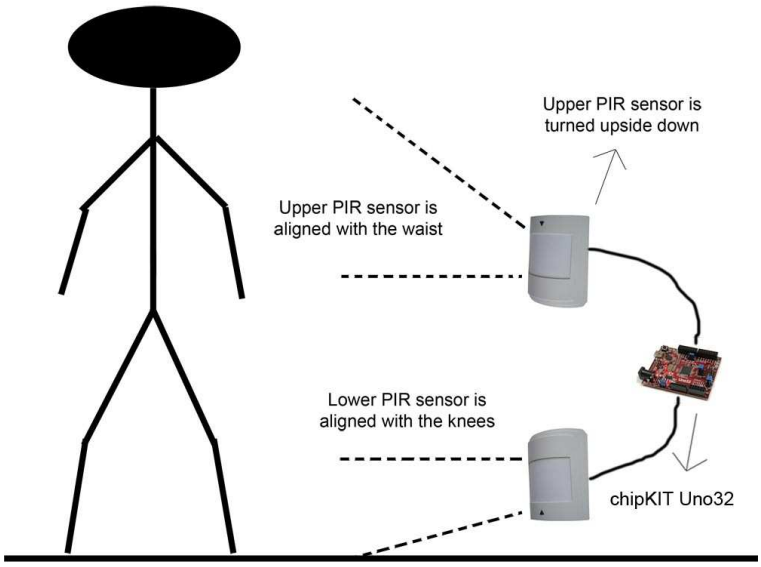

Figure 4.5: A walking man illustration to describe working mechanism of the two-PIR-sensor based falling person detection system.

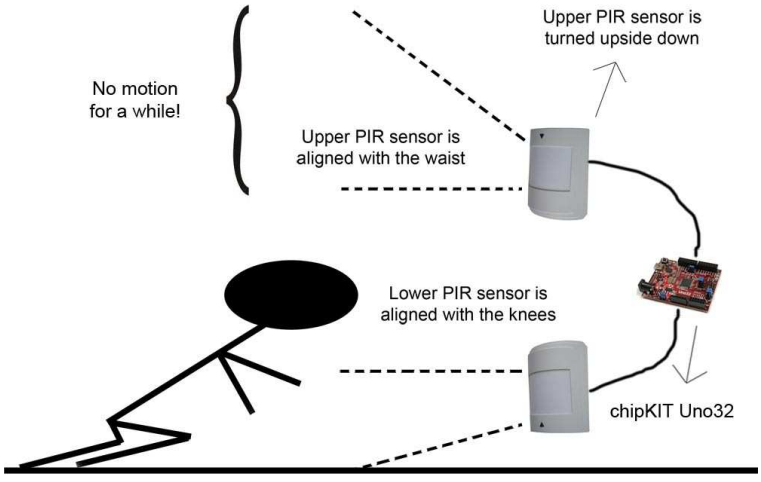

Figure 4.6: A falling man illustration to describe working mechanism of the two-PIR-sensor based falling person detection system.

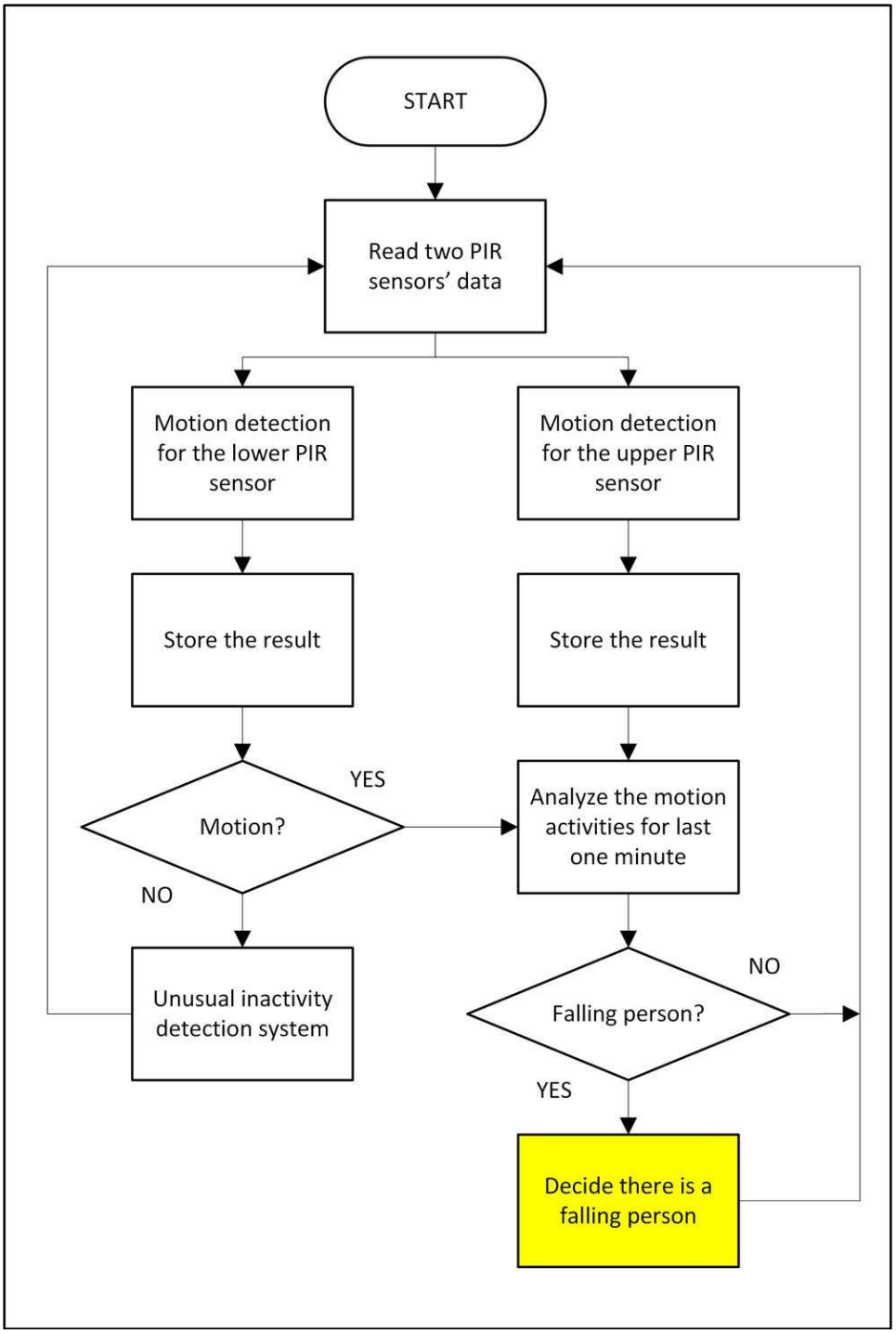

Figure 4.7: Flowchart of the two-PIR-sensor based falling person detection algorithm.

Table 4.11: Confusion matrix for the two-PIR-sensor based falling person detection system using the second dataset. This dataset is composed of one-minute-long records which correspond to the one sample for every one minute.

Actual Class	Predicted Class	
	Other Sources	**Falling Person**
Other Sources	38	2
Falling Person	5	15

Confusion matrix for the two-PIR-sensor based system is presented in Table 4.11. There are some miss-detections in the experimental results. The main reason for these miss-detections is instant fallings which may not be detected if the person faints and there is not any human motion in the lower PIR sensor for a while. The other miss-detections are caused by the case that the falling person makes an effort to stand up but he/she does not succeed. Therefore, the upper PIR sensor detects motion and the falling event may not be detected in one minute. Besides, false alarms are caused by sitting on the floor for a while.

Some other example situations are illustrated in Figure 4.8 and 4.9. If a person sitting in the room, the upper PIR sensor can detect motions of the head and shoulders of the person. By this way, the system can know that the person is not on the floor. As another example, if the person sleeps on his/her bed, the lower PIR sensor does not detect any human motion and the system can decide there is not a falling person. Additionally, if a person stands up healthy after a falling event, the two-PIR-sensor based system can detect it and cancel the emergency alarm.

A significant advantage of the two-PIR-sensor based system is that it is not affected by the person or the environment. Besides, the sensor signals can be analyzed as a process and different algorithms can be developed more easily. Currently, the prominent disadvantage of two-PIR-sensor based system is that it can not detect instant falling events which are ended up with a fainting.

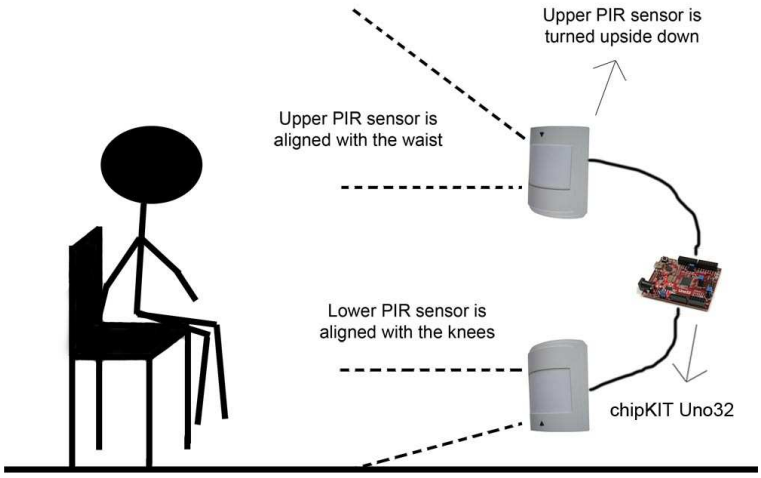

Figure 4.8: A sitting man illustration to describe working mechanism of the two-PIR-sensor based falling person detection system.

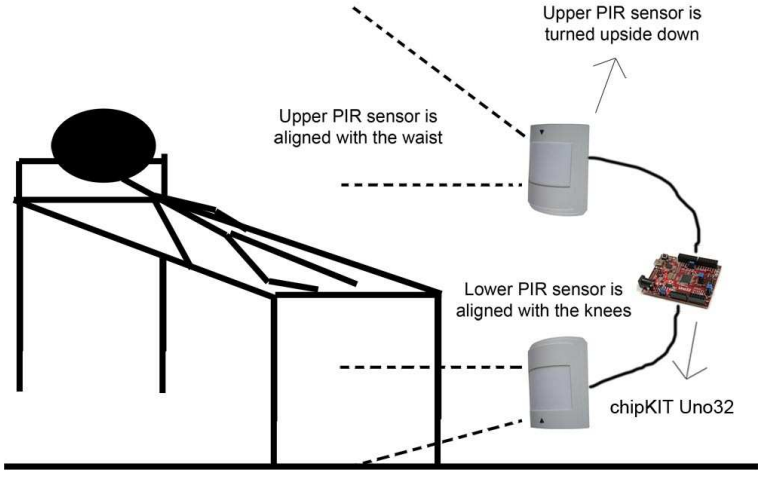

Figure 4.9: A sleeping man illustration to describe working mechanism of the two-PIR-sensor based falling person detection system.

Table 4.12: Confusion matrix for the multi-sensor based falling person detection system using the second dataset. This dataset is composed of one-minute-long records which correspond to the one sample for every one minute.

Actual Class	Predicted Class	
	Other Sources	**Falling Person**
Other Sources	38	2
Falling Person	0	20

4.3.3 Multi-Sensor Based Detection Algorithm

As emphasized before, achievement of zero miss-detection rate is crucial for the falling person detection systems. Therefore, the vibration sensor and two PIR sensors are employed together for the purpose of achievement of zero miss-detection rate. Flowchart of the multi-sensor based algorithm is presented in Figure 4.10. The vibration sensor based and the two-PIR-sensor based algorithms are run serially to make a final decision for the falling event. These two falling person detection systems are complementary for each other. Hence, the miss-detection rate is decreased using multi-sensor based system as it can be seen from Table 4.12.

If the vibration sensor based system finds candidate fall regions, two result vectors of the two-PIR-sensor based system are reseted. Hence, the two-PIR-sensor based system can chase the event more carefully by focusing the after of the event. As an another situation, if the vibration sensor based system detects certain falling event, the final decision is made without looking the results of two-PIR-sensor based system. By this way, instant fallings can be detected. On the contrary, slow fallings can be detected by the two-PIR-sensor based system without considering the vibration-sensor based system. Since, there is not any chance to analyze the falling event if the vibration is not sensed on the floor by the vibration sensor based system but the two-PIR-sensor based system can detect this falling anyway. Additionally, any falling alarm can be canceled if the two-PIR-sensor based system decides that there is a walking person in the room.

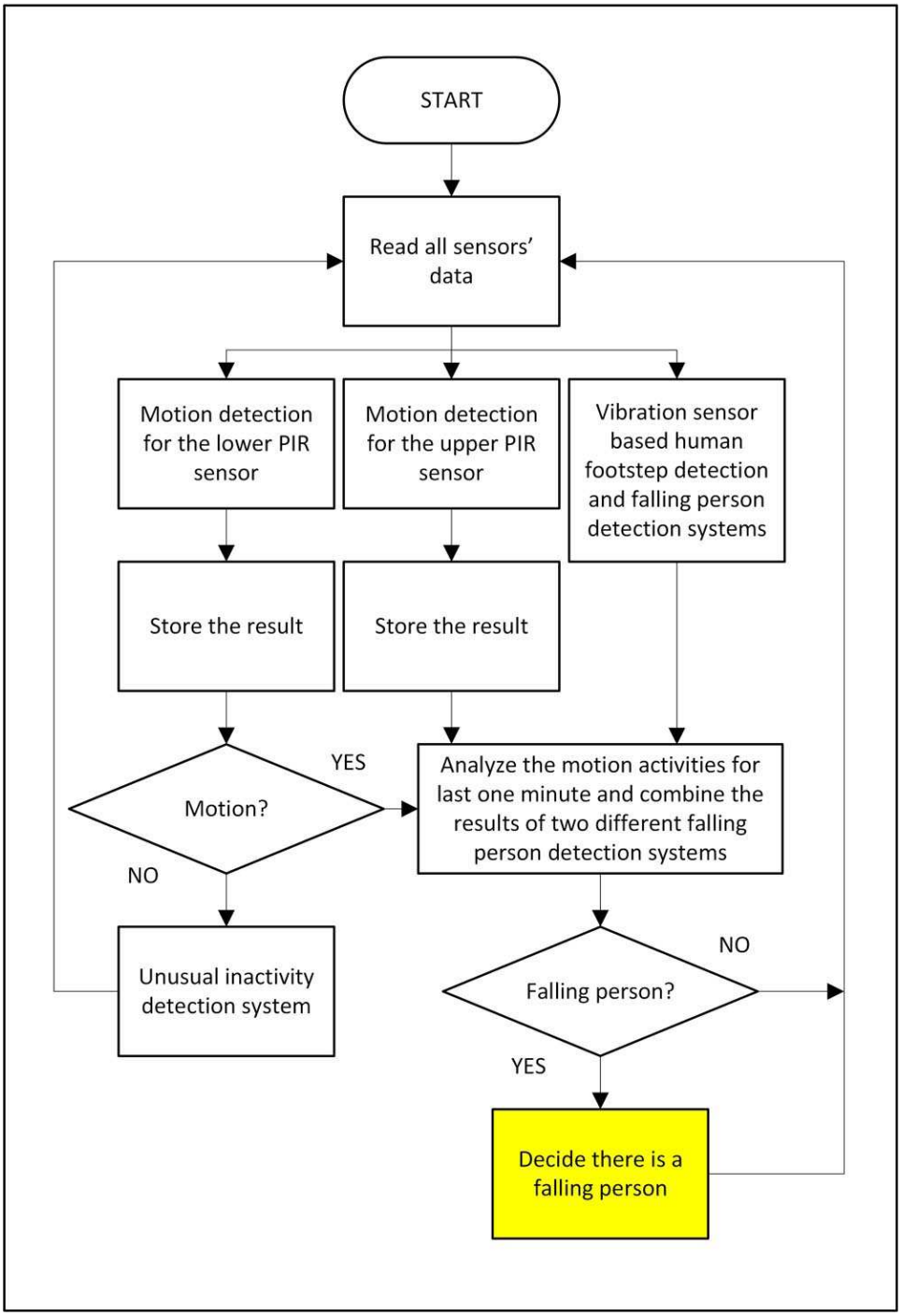

Figure 4.10: Flowchart of the multi-sensor based falling person detection algorithm.

Table 4.13: Confusion matrix for the vibration sensor based indoor flooding detection system.

Actual Class	Predicted Class	
	No Activity	**Running Water**
No Activity	75	1
Running Water	0	47

4.4 Indoor Flooding Detection

The main purpose of the indoor flooding detection systems is to prevent taps stay open without an intention because elderly people may forget to close the taps in a house. In this thesis, the PIR sensor is tested to see how the sensor signal is changing when there is a running water. It is understood from the tests, a remarkable variation does not happened for the PIR sensor signal while the water is running from the tap. The PIR sensor signal only differs when the hot water starts to flow but it is not enough for an indoor flooding detection system.

If an open tap is forgotten, the running water fills the sink after a while and the water starts to drop onto the floor. Considering this situation, the vibration sensor based system is developed to detect indoor flooding by taking advantage of vibrations caused by water drops on the floor. The vibration sensor signals are recorded while there is not any other signal sources except water drops. It is assumed that the person is not in a bathroom while the water is running and if the person enters the bathroom, the system is deactivated.

For the classification, an adaptive-threshold based method is employed using Eq. 4.1 and 4.2. In the experimental results shown in Table 4.13, α and β are selected as 0.6 and 1.8, respectively. T_a is set to 2 for the beginning and this threshold is updated by analyzing the variance of the 1024-sample-long vibration sensor signal windows. If the variance of the signal window exceeds the adaptive threshold, it is judged that there is an indoor flooding.

4.5 Stand-Alone Sensor Fusion Application

After the MATLAB implementations of the all detection systems, a stand-alone application is developed using chipKIT Uno32 boards and real-time experiments are carried out in the laboratory environment. Each one of the sensors is connected to a separate Uno32 board and a network is established among the Uno32 boards. At the end of this network, there is a main processor unit which is an also Uno32 board. The main processor fuses the subsystem decisions to send an appropriate alarm to desired emergency units.

In our implementation, Uno32 boards communicate using Cat 5 cables and the 12 V electricity is also provided through the Cat 5 cables. Three bits of data is transmitted by the digital I/O pins of consecutive Uno32 boards. Each of the Uno32 boards checks the detection results of the previous Uno32 board and transmits the fused results by adding new detection results of itself to the next Uno32 board. Flowcharts for the activity-output relation using three bits of data are presented in Figure 4.11 and 4.12 based on the vibration sensor and two PIR sensors, respectively. As it can be seen, activities have different priorities according to the importance degree of the emergency situation. For an example, if a falling person is detected, the other alarms are ignored. The output bits are obtained by the following conditions:

- Vibration sensor related situation; falling person is detected -> 011
- Vibration sensor related situation; indoor flooding is detected -> 010
- Vibration sensor related situation; human footstep is detected -> 001
- Vibration sensor related situation; no activity -> 000
- PIR sensor related situation; falling person is detected -> 111
- PIR sensor related situation; uncontrolled flame is detected -> 110
- PIR sensor related situation; human motion activity is detected -> 101
- PIR sensor related situation; no activity -> 100

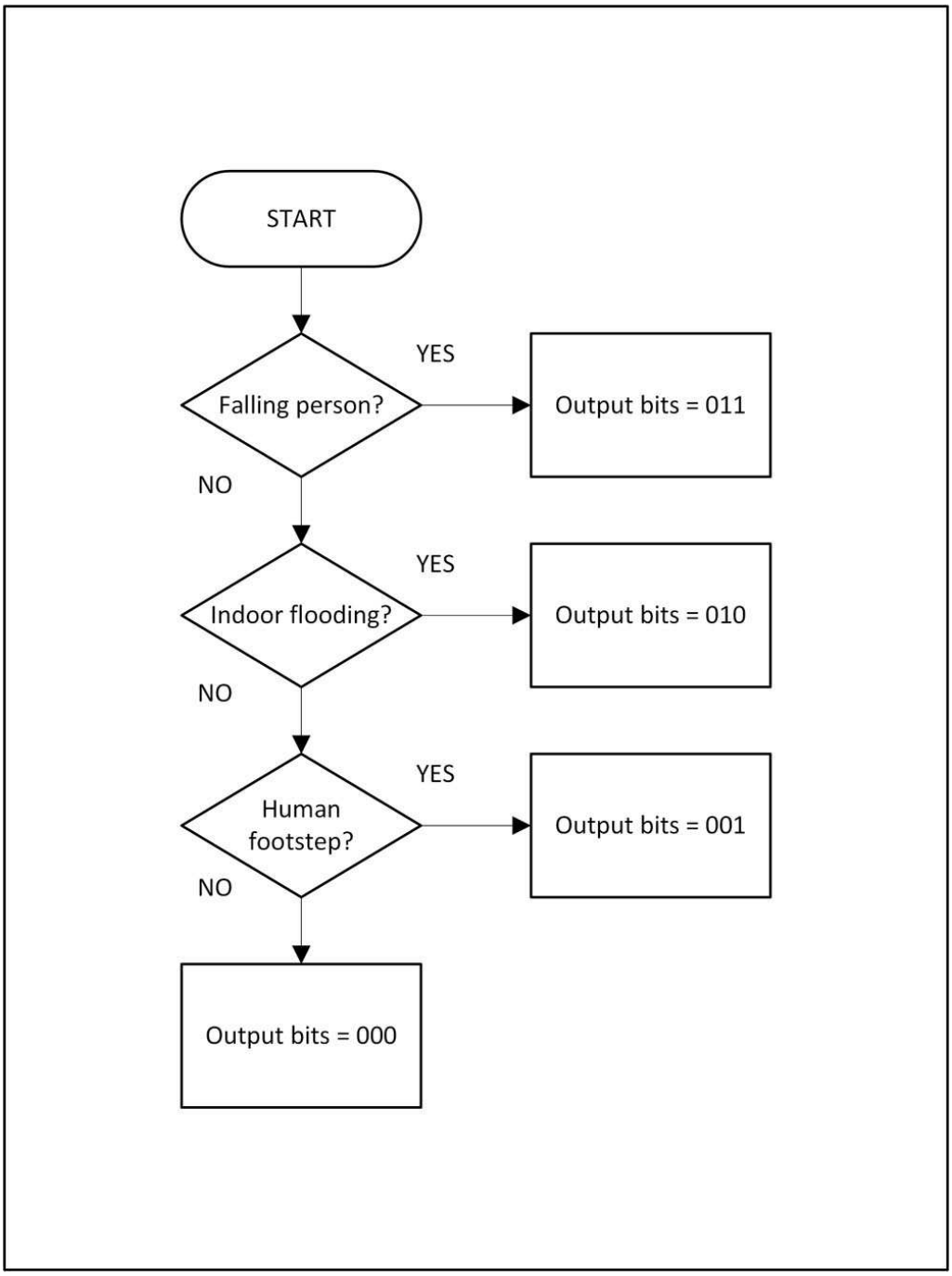

Figure 4.11: Flowchart for the vibration sensor based activity-output relation using three bits of data.

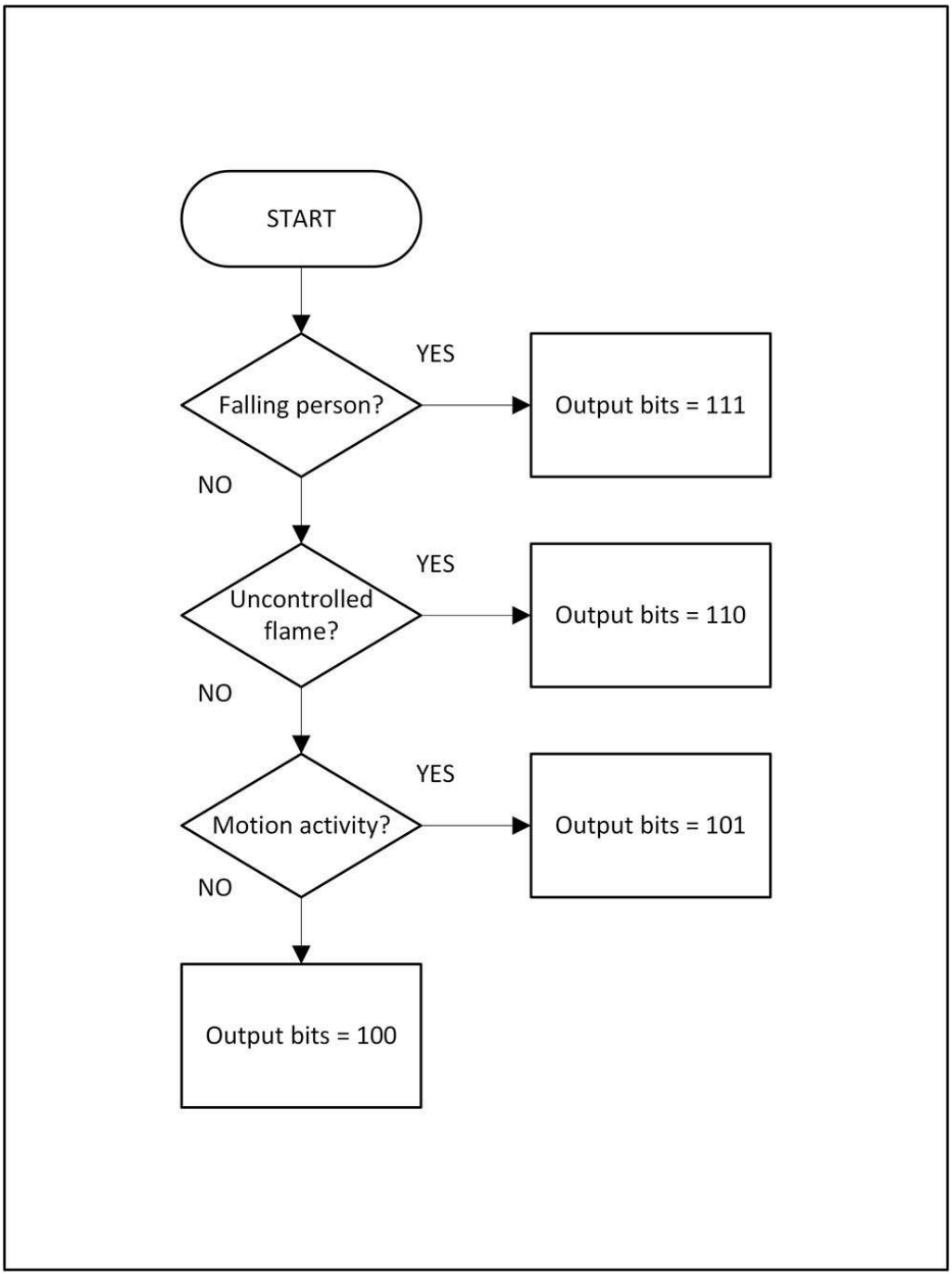

Figure 4.12: Flowchart for the two-PIR-sensor based activity-output relation using three bits of data.

By the way, the uncontrolled flame detection system using a similar algorithm with the MM based classifier is integrated to our embedded system [57]. The PIR sensor based uncontrolled flame detection system does not give an alarm if there is a controlled flame like a gas cooker flame. Because, the controlled flames do not effect the PIR sensor signal significantly. It is reported that uncontrolled flames flicker with a frequency of around 10 Hz [77]. Therefore, uncontrolled flames can be detected benefiting from this information and using the PIR sensor.

In Figure 4.13, an illustration for the dataflow between Uno32 boards using three bits of data is presented. It can be seen from the illustration, the dataflow starts from the vibration sensors and follows a way to the main processor through the PIR sensors. Two vibration sensors are enough for an average size home and there are dataflow loops in the number of the vibration sensors. Hence, two dataflow loops are employed in our example and the main processor decides which type of an alarm is given in the end.

In our stand-alone system, a low-cost simple conductivity based circuit is used to detect indoor flooding instead of the vibration sensor based system. The vibration sensor based system can detect the indoor flooding if there is not any vibration signal sources in the environment but otherwise there may be false alarms. Hence, a low-cost simple conductivity based indoor flooding detector is integrated to our embedded system. The main principle of this simple detector is that if the two wires are short circuited by the water, transmits the logic one to the related processor. Therefore, the indoor flooding detector circuit is connected to the Uno32 board which is also used for the vibration sensor signal processing.

An example smart home environment which has two vibration sensors, eight pair PIR sensors, and three flooding detectors is illustrated in Figure 4.14. As emphasized before, it is assumed that only one person lives in a smart home for our designs. And, neighbors can be considered as another vibration signal sources. Therefore, vibration sensors should be placed as far away from the neighbors as possible. In the example illustration, the vibration sensors are located in a hall of the house. Two PIR sensors (pair PIR sensors) are placed in each room by covering the whole room.

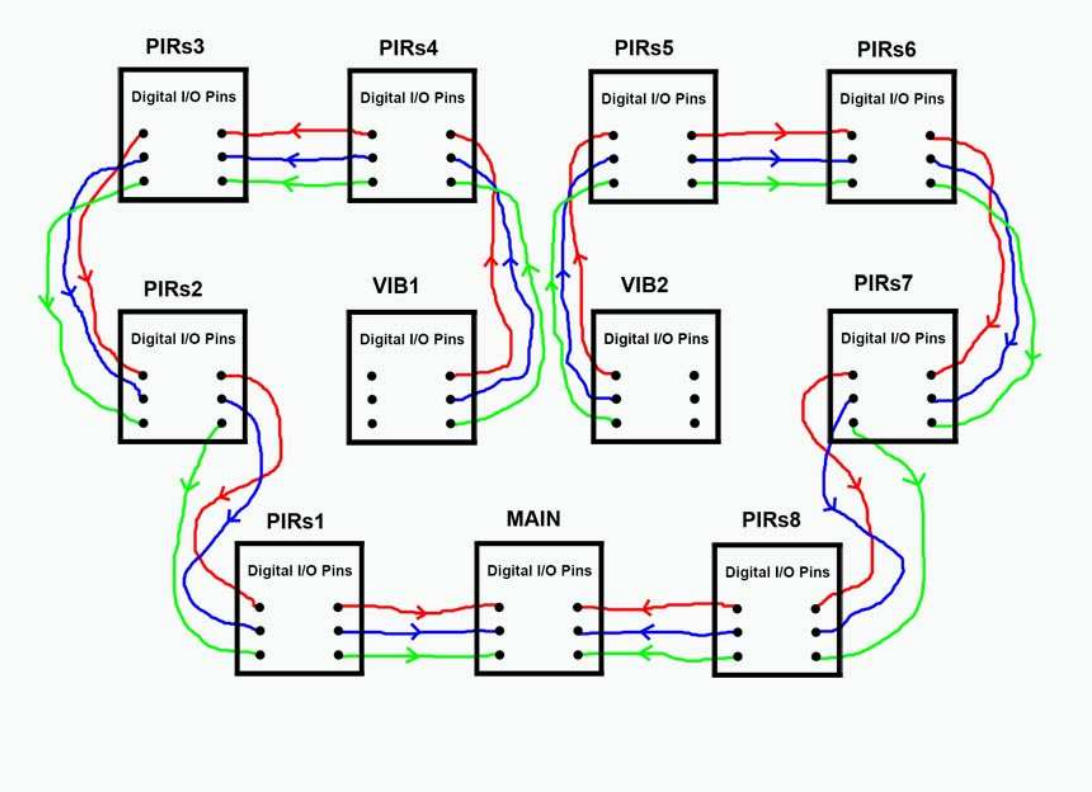

Figure 4.13: Illustration for the dataflow between Uno32 boards using three bits of data.

The main processor fuses the subsystem decisions to make final decisions. For an example, results of the two falling person detection systems are fused in the main processor. Somehow, if the falling event is missed, the unusual inactivity detection system can be employed as a supplementary system to guarantee to give an alarm a little lately. Additionally, a button circuit near a bed can be used to inactivate the unusual inactivity detection system during sleeping time.

As a final subject, if there is a pet at home then it can be detected. It is possible to distinguish walking pets from human beings using the PIR sensor signal, because leg movements of pets are much frequent than human beings [20]. By this way, movements of pet can be ignored to prevent possible complications. The pet movement detection system will be integrated to the AAL system later.

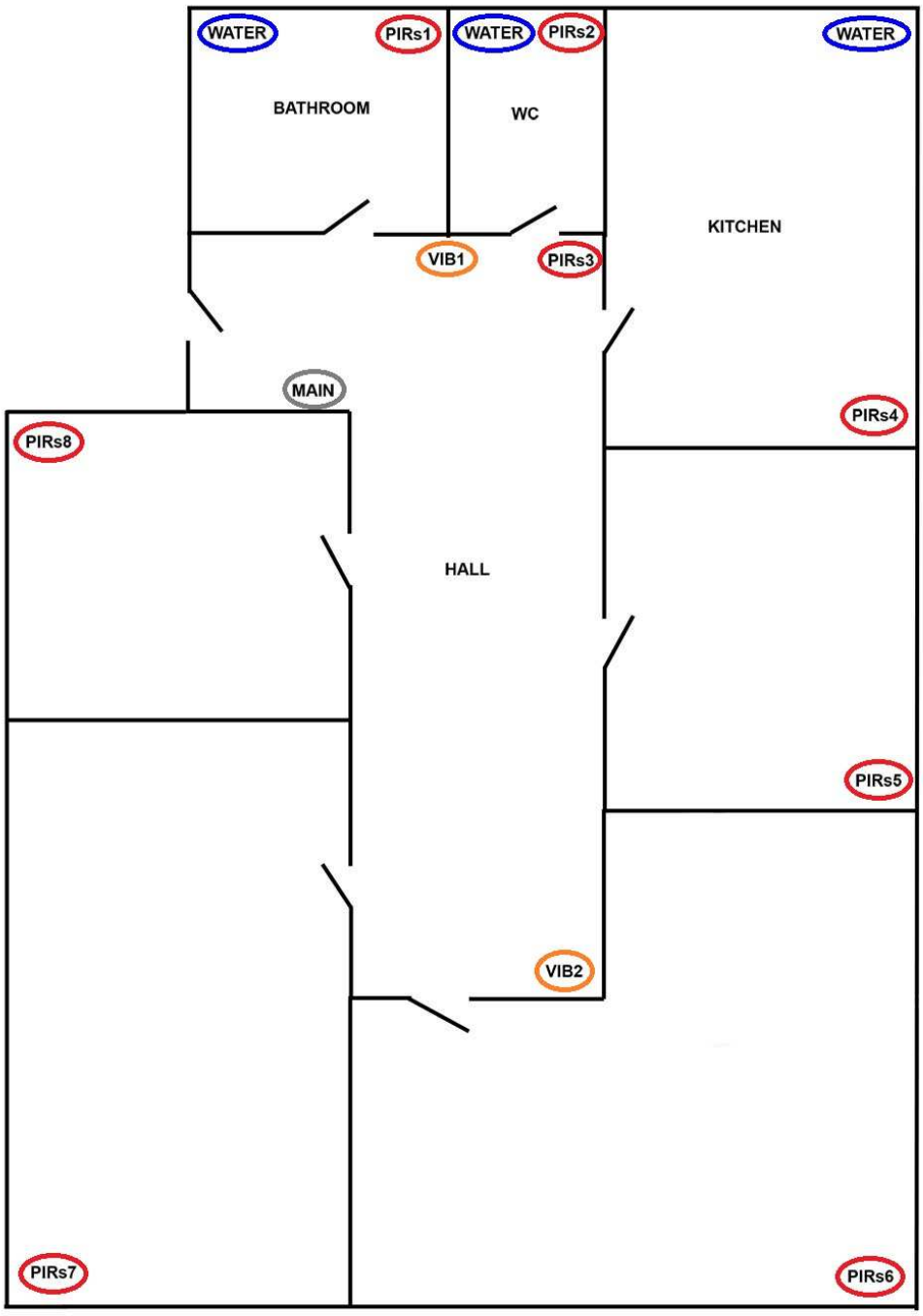

Figure 4.14: An example smart home environment which has two vibration sensors, eight pair PIR sensors, and three flooding detector circuits.

4.6 Summary

Our vibration sensor based falling person detection application may not be an appropriate example to show the desirable properties of the DT-$\mathbb{C}$WT and the ST-$\mathbb{C}$WT such as shift-invariance and lack of aliasing. Because, the energies of the frequency sub-bands are used as feature parameters and the fine details of the frequency content does not effect the overall sub-band energies. However, it is experimentally observed that the ST-$\mathbb{C}$WT method can be applied to vibration sensor signal processing applications instead of the computationally expensive DT-$\mathbb{C}$WT.

An AAL system using the vibration and two PIR sensors is developed in a stand-alone structure. The vibration sensor is employed for the falling person detection, human footstep detection, and indoor flooding detection. Two PIR sensors are employed for the falling person detection, human motion detection, unusual inactivity detection, and uncontrolled flame detection. Pet movement detection and gas leak detection systems will be integrated to our embedded system in the future. The emergency alarms are transmitted to the emergency units through the auto-dial alarm system which is connected to the stand-alone system.

Some novel algorithms are developed for the detection systems and our theoretical studies are employed in these detection systems. Different feature extraction methods, different classifiers, and different algorithms can be tested for the aforesaid detection systems. As an example, our simple two-PIR-sensor based falling person detection algorithm can be improved in many ways and a better system can be designed without making a big effort. Besides, different hardwares also can be tested. For an another example, we used Uno32 boards however cheaper PIC microcontrollers also can be employed for a similar stand-alone system design. In additionally, our stand-alone system can be modernized using wireless modules and rechargeable batteries in the future.

Chapter 5

Conclusion and Future Work

In this thesis, an AAL system application which employs vibration and PIR sensors is presented. The goal is to design an AAL system for elderly and handicapped people.

Various frequency analysis methods which consist of the DFT, MFCC, DWT with different filter-banks, DT-$\mathbb{C}$WT and ST-$\mathbb{C}$WT are studied for vibration sensor signal processing. Different datasets are formed using the sensors. Feature extraction and classification methods for the human footstep detection, falling person detection, and indoor flooding detection using the vibration sensor are proposed. One PIR sensor is employed to detect human motion and unusual inactivity detection, and two PIR sensors are employed in falling person detection. The multi-sensor based falling person detection system is also designed using the vibration and two PIR sensors. Some novel algorithms are introduced in these detection algorithms. The PIR sensor based uncontrolled flame detection system is integrated to the overall system. The prototype AAL system is constructed using Uno32 boards instead of personal computers to reduce costs. A network is setup for the communication of the Uno32 boards which are connected to different sensors. The main processor gives final decisions, and emergency alarms are transmitted to a call center or to another telephone number using the auto-dial alarm system.

As a future work, there may be several studies that include hardware related, theoretical, and application related studies. For the hardware related studies, different vibration sensors can be tested to see which one is more appropriate to use in a house. Besides, the existing hard-wired networking system can be converted to a wireless one using ZigBee modules. Additionally, rechargeable batteries can be placed alongside the Uno32 boards and different processor units also can be selected instead of the Uno32 boards. Power consumption may be calculated and energy-efficient systems can be designed for the overall AAL system.

The ST-$\mathbb{C}$WT filter coefficients are computed considering the perfect reconstruction conditions. However, perfect reconstruction examples are not examined for the ST-$\mathbb{C}$WT and perfect reconstruction based comparison is not included in this thesis. Therefore, reconstruction experiments can be conducted to test the lack of aliasing property for the wavelet-based signal analysis methods in the future.

For the future applications, a larger dataset is essential. This dataset should include various records which contain different human activities from many people and houses. It will be also desirable to have data from handicapped people using wheelchairs and canes. Additionally, analyzing motion activities of sleeping people is an important study to handle possible problems.

Different adaptive systems for the vibration sensor signal is an another subject to study. More sensitive human footstep detection systems can be developed. Various feature extraction and classification methods can be applied and compared to each other in all subsystems. Optimization of the signal windows' lengths for the detection systems can be a useful study. Developing different algorithms can be a solution for the false alarm sources. Lastly, previous studies about pet movement detection and gas leak detection subsystems will be integrated to the overall AAL system in the future.

Bibliography

[1] J. M. Hausdorff, D. A. Rios, and H. K. Edelberg, "Gait Variability and Fall Risk in Community-Living Older Adults: A 1-year Prospective Study," *Archives of Physical Medicine and Rehabilitation*, vol. 82, pp. 1050–1056, Aug. 2001.

[2] V. Ricquebourg, D. Menga, D. Durand, B. Marhic, L. Delahoche, and C. Loge, "The Smart Home Concept: Our Immediate Future," in *IEEE 1st International Conference on E-Learning in Industrial Electronics*, pp. 23–28, Dec. 2006.

[3] Q. C. Nguyen, D. Shin, D. Shin, and J. Kim, "Real-Time Human Tracker Based on Location and Motion Recognition of User for Smart Home," in *IEEE 3rd International Conference on Multimedia and Ubiquitous Engineering (MUE-2009)*, pp. 243–250, Jun. 2009.

[4] B. U. Toreyin, Y. Dedeoglu, and A. E. Cetin, "HMM Based Falling Person Detection Using Both Audio and Video," *Computer Vision in Human-Computer Interaction, Lecture Notes in Computer Science*, vol. 3766, pp. 211–220, Oct. 2005.

[5] A. Ben Hadj Mohamed, T. Val, L. Andrieux, and A. Kachouri, "Using a Kinect WSN for Home Monitoring: Principle, Network and Application Evaluation," in *IEEE International Conference on Wireless Communications in Unusual and Confined Areas (ICWCUCA-2012)*, pp. 1–5, Aug. 2012.

[6] G. Mastorakis and D. Makris, "Fall Detection System Using Kinect's Infrared Sensor," *Journal of Real-Time Image Processing*, pp. 1–12, Mar. 2012.

[7] K. Altun, B. Barshan, and O. Tuncel, "Comparative Study on Classifying Human Activities with Miniature Inertial and Magnetic Sensors," *Pattern Recognition*, vol. 43, pp. 3605–3620, Oct. 2010.

[8] A. Yurtman and B. Barshan, "Investigation of Personal Variations in Activity Recognition Using Miniature Inertial Sensors and Magnetometers," in *IEEE 20th Signal Processing and Communications Applications Conference (SIU-2012)*, pp. 1–4, Apr. 2012.

[9] M. N. Nyan, F. E. H. Tay, and E. Murugasu, "A Wearable System for Pre-Impact Fall Detection," *Journal of Biomechanics*, vol. 41, pp. 3475–3481, Dec. 2008.

[10] G. R. Yavuz, H. Yalcin, L. Akarun, and C. Ersoy, "Wavelet Transform Based Fall Detection," in *IEEE 19th Signal Processing and Communications Applications (SIU-2011)*, pp. 142–145, Apr. 2011.

[11] K. N. Ha, K. C. Lee, and S. Lee, "Development of PIR Sensor Based Indoor Location Detection System for Smart Home," in *IEEE International Joint Conference (SICE-ICASE-2006)*, pp. 2162–2167, Oct. 2006.

[12] M. Usman, V. Muthukkumarasamy, X.-W. Wu, and S. Khanum, "Wireless Smart Home Sensor Networks: Mobile Agent Based Anomaly Detection," in *Ubiquitous Intelligence Computing and IEEE 9th International Conference on Autonomic and Trusted Computing (UIC/ATC-2012)*, pp. 322–329, Sept. 2012.

[13] H. Zheng, H. Wang, and N. Black, "Human Activity Detection in Smart Home Environment with Self-Adaptive Neural Networks," in *IEEE International Conference on Networking, Sensing and Control (ICNSC-2008)*, pp. 1505–1510, Apr. 2008.

[14] C. Zhang, M. Zhang, Y. Su, and W. Wang, "Smart Home Design Based on ZigBee Wireless Sensor Network," in *IEEE 7th International ICST Conference on Communications and Networking in China (CHINACOM-2012)*, pp. 463–466, Aug. 2012.

[15] M. Mubashir, L. Shao, and L. Seed, "A Survey on Fall Detection: Principles and Approaches," *Neurocomputing, Behaviours in Video*, vol. 100, pp. 144–152, Jan. 2013.

[16] F. Marquis-Faulkes, S. J. McKenna, P. Gregor, and A. F. Newell, "Scenario-Based Drama as a Tool for Investigating User Requirements with Application to Home Monitoring for Elderly People," in *10th International Conference on Human-Computer Interaction (HCI-2003)*, pp. 512–516, Jun. 2003.

[17] H. Nait-Charif and S. J. McKenna, "Activity Summarisation and Fall Detection in a Supportive Home Environment," in *IEEE 17th International Conference on Pattern Recognition (ICPR-2004)*, vol. 4, pp. 323–326, Aug. 2004.

[18] S. Brownsell, D. Bradley, F. Cardinaux, and M. Hawley, "Developing a Systems and Informatics Based Approach to Lifestyle Monitoring within eHealth: Part I - Technology and Data Management," in *IEEE 1st International Conference on Healthcare Informatics, Imaging and Systems Biology (HISB-2011)*, pp. 264–271, Jul. 2011.

[19] J. Dai, X. Bai, Z. Yang, Z. Shen, and D. Xuan, "Mobile Phone-Based Pervasive Fall Detection," *Personal and Ubiquitous Computing*, vol. 14, pp. 633–643, Oct. 2010.

[20] B. U. Toreyin, E. B. Soyer, I. Onaran, and A. E. Cetin, "Falling Person Detection Using Multi-Sensor Signal Processing," *EURASIP Journal Advances in Signal Processing*, vol. 2008, pp. 1–7, Jan. 2008.

[21] M. Alwan, P. J. Rajendran, S. Kell, D. Mack, S. Dalal, M. Wolfe, and R. Felder, "A Smart and Passive Floor-Vibration Based Fall Detector for Elderly," in *IEEE 2nd International Conference on Information and Communication Technologies: From Theory to Applications (ICTTA-2006)*, vol. 1, pp. 1003–1007, Apr. 2006.

[22] X. Luo, T. Liu, J. Liu, X. Guo, and G. Wang, "Design and Implementation of a Distributed Fall Detection System Based on Wireless Sensor Networks," *EURASIP Journal on Wireless Communications and Networking*, Mar. 2012.

[23] T. Liu, X. Guo, and G. Wang, "Elderly-Falling Detection Using Distributed Direction-Sensitive Pyroelectric Infrared Sensor Arrays," *Multidimensional Systems and Signal Processing*, vol. 23, pp. 451–467, Dec. 2012.

[24] I. Bouchrika, J. Carter, M. Nixon, R. Morzinger, and G. Thallinger, "Using Gait Features for Improving Walking People Detection," in *IEEE 20th International Conference on Pattern Recognition (ICPR-2010)*, pp. 3097–3100, Aug. 2010.

[25] H.-F. Xing, F. Li, and Y.-L. Liu, "Wavelet Denoising and Feature Extraction of Seismic Signal for Footstep Detection," in *IEEE International Conference on Wavelet Analysis and Pattern Recognition (ICWAPR-2007)*, vol. 1, pp. 218–223, Nov. 2007.

[26] V. V. Reddy, V. Divya, A. W. H. Khong, and B. P. Ng, "Footstep Detection and Denoising Using a Single Triaxial Geophone," in *IEEE Asia Pacific Conference on Circuits and Systems (APCCAS-2010)*, pp. 1171–1174, Dec. 2010.

[27] A. Pakhomov and T. Goldburt, "New Seismic Sensors for Footstep Detection and Other Military Applications," *Sensors, and Command, Control, Communications, and Intelligence (C3I) Technologies for Homeland Security and Homeland Defense III*, vol. 5403, pp. 463–468, 2004.

[28] M. Mathie, A. Coster, N. Lovell, and B. Celler, "Detection of Daily Physical Activities Using a Triaxial Accelerometer," *Medical and Biological Engineering and Computing*, vol. 41, no. 3, pp. 296–301, 2003.

[29] S. Bouchafa, D. Aubert, and S. Bouzar, "Crowd Motion Estimation and Motionless Detection in Subway Corridors by Image Processing," in *IEEE Conference on Intelligent Transportation System (ITSC-1997)*, pp. 332–337, Nov. 1997.

[30] S. Zhang, P. McCullagh, C. Nugent, and H. Zheng, "A Theoretic Algorithm for Fall and Motionless Detection," in *IEEE 3rd International Conference on Pervasive Computing Technologies for Healthcare, (PervasiveHealth-2009)*, pp. 1–6, Apr. 2009.

[31] B. Taati, J. Snoek, D. Giesbrecht, and A. Mihailidis, "Water Flow Detection in a Handwashing Task," in *IEEE Canadian Conference on Computer and Robot Vision (CRV-2010)*, pp. 175–182, Jun. 2010.

[32] W. Sweldens, "The Lifting Scheme: A New Philosophy in Biorthogonal Wavelet Constructions," in *Wavelet Applications in Signal and Image Processing III*, pp. 68–79, Sept. 1995.

[33] M. F. Keskin, "Image Processing Methods for Computer-Aided Interpretation of Microscopic Images," Master's thesis, Bilkent University, 2012.

[34] A. Abbas and T. D. Tran, "Rational Coefficient Dual-Tree Complex Wavelet Transform: Design and Implementation," *IEEE Transactions on Signal Processing*, vol. 56, pp. 3523–3534, Aug. 2008.

[35] A. Eleyan, H. Ozkaramanli, and H. Demirel, "Complex Wavelet Transform-Based Face Recognition," *EURASIP Journal on Advances in Signal Processing*, vol. 2008, pp. 1–13, Jan. 2008.

[36] D. Mellis, M. Banzi, D. Cuartielles, and T. Igoe, "Arduino: An Open Electronics Prototyping Platform," in *25th Conference on Human Factors in Computing (CHI-2007)*, 2007.

[37] Digilent Inc., "chipKIT Uno32 Board Reference Manual," Datasheet 502–209, Digilent Inc., Revision: October 26, 2012.

[38] E. Clements, "Good Vibrations at Fermilab," *The Newsletter of the Linear Collider Community*, August 9, 2007.

[39] ION Geophysical Corporation, "Geophones," Datasheet 1–12, ION Geophysical Corporation, 2006.

[40] K. M. Houston and D. P. McGaffigan, "Spectrum Analysis Techniques for Personnel Detection Using Seismic Sensors," *Unattended Ground Sensor Technologies and Applications V*, vol. 5090, pp. 162–173, 2003.

[41] E. R. Ranger, "Demonstration System for a Low-Power Seismic Detector and Classifier," Master's thesis, Massachusetts Institute of Technology, 2003.

[42] A. Sundaresan, A. Subramanian, P. K. Varshney, and T. Damarla, "A Copula-Based Semi-Parametric Approach for Footstep Detection Using Seismic Sensor Networks," *Multisensor, Multisource Information Fusion: Architectures, Algorithms, and Applications*, vol. 7710, pp. 1–12, 2010.

[43] R. Haff and T. Pearson, "Separating In-Shell Pistachio Nuts from Kernels Using Impact Vibration Analysis," *Sensing and Instrumentation for Food Quality and Safety*, vol. 1, pp. 188–192, Aug. 2007.

[44] R. Bajwa, R. Rajagopal, P. Varaiya, and R. Kavaler, "In-Pavement Wireless Sensor Network for Vehicle Classification," in *IEEE 10th International Conference on Information Processing in Sensor Networks (IPSN-2011)*, pp. 85–96, Apr. 2011.

[45] D. Anderson, "Optical Fiber Sensors for Perimeter and IT Protection," Application Notes FSI TP 02, Fiber SenSys, 2012.

[46] Glolab Corporation, "How Infrared Motion Detector Components Work," Application Notes, Glolab Corporation, NY, USA, 2013.

[47] T. M. Hussain, A. M. Baig, T. N. Saadawi, and S. A. Ahmed, "Infrared Pyroelectric Sensor for Detection of Vehicular Traffic Using Digital Signal Processing Techniques," *IEEE Transactions on Vehicular Technology*, vol. 44, no. 3, pp. 683–689, 1995.

[48] C.-H. Tsai, Y.-W. Bai, C.-A. Chu, C.-Y. Chung, and M.-B. Lin, "PIR-Sensor-Based Lighting Device with Ultra-Low Standby Power Consumption," *IEEE Transactions on Consumer Electronics*, vol. 57, no. 3, pp. 1157–1164, 2011.

[49] L.-W. Hung, H.-H. Lai, C.-L. Chuang, and C.-L. Lu, "An Intelligent Lighting System for Exhibition Applications," in *IEEE International Conference on Consumer Electronics, Communications and Networks (CECNet-2011)*, pp. 4748–4750, Apr. 2011.

[50] Y.-W. Bai and Y.-T. Ku, "Automatic Room Light Intensity Detection and Control Using a Microprocessor and Light Sensors," *IEEE Transactions on Consumer Electronics*, vol. 54, pp. 1173–1176, Aug. 2008.

[51] M. Moghavvemi and L. C. Seng, "Pyroelectric Infrared Sensor for Intruder Detection," in *IEEE Region 10 Conference (TENCON-2004)*, vol. 4, pp. 656–659, Nov. 2004.

[52] The SmartDetect WSN Team, "SmartDetect: An Efficient WSN Implementation for Intrusion Detection," in *IEEE 2nd International Conference on Communication Systems and Networks (COMSNETS-2010)*, Jan. 2010.

[53] G. Feng, M. Liu, X. Guo, J. Zhang, and G. Wang, "Genetic Algorithm Based Optimal Placement of PIR Sensor Arrays for Human Localization," in *IEEE International Conference on Mechatronics and Automation (ICMA-2011)*, pp. 1080–1084, Aug. 2011.

[54] Q. Hao, F. Hu, and J. Lu, "Distributed Multiple Human Tracking with Wireless Binary Pyroelectric Infrared (PIR) Sensor Networks," in *IEEE Sensors*, pp. 946–950, Nov. 2010.

[55] F. Wahl, M. Milenkovic, and O. Amft, "A Distributed PIR-Based Approach for Estimating People Count in Office Environments," in *IEEE/IFIP 10th International Conference on Embedded and Ubiquitous Computing (EUC-2012)*, pp. 640–647, Dec. 2012.

[56] T. Yokoishi, J. Mitsugi, O. Nakamura, and J. Murai, "Room Occupancy Determination with Particle Filtering of Networked Pyroelectric Infrared (PIR) Sensor Data," in *IEEE Sensors*, pp. 1–4, Oct. 2012.

[57] F. Erden, B. U. Toreyin, E. B. Soyer, I. Inac, O. Gunay, K. Kose, and A. E. Cetin, "Wavelet Based Flame Detection Using Differential PIR Sensors," in *IEEE 20th Signal Processing and Communications Applications Conference (SIU-2012)*, pp. 1–4, Apr. 2012.

[58] F. Erden, E. B. Soyer, B. U. Toreyin, and A. E. Cetin, "VOC Gas Leak Detection Using Pyro-Electric Infrared Sensors," in *IEEE International Conference on Acoustics Speech and Signal Processing (ICASSP-2010)*, pp. 1682–1685, Mar. 2010.

[59] F. R. M. Rashidi, M. H. Ariff, and M. Z. Ibrahim, "Car Monitoring Using Bluetooth Security System," in *IEEE International Conference on Electrical, Control and Computer Engineering (INECCE-2011)*, pp. 424–428, Jun. 2011.

[60] Holtek Semiconductor Inc., "HT9200A/HT9200B DTMF Generators," Datasheet Rev. 1.41, Holtek Semiconductor Inc., 2009.

[61] I. W. Selesnick, R. G. Baraniuk, and N. C. Kingsbury, "The Dual-Tree Complex Wavelet Transform," *IEEE Signal Processing Magazine*, vol. 22, pp. 123–151, Nov. 2005.

[62] F. Jabloun, A. E. Cetin, and E. Erzin, "Teager Energy Based Feature Parameters for Speech Recognition in Car Noise," *IEEE Signal Processing Letters*, vol. 6, pp. 259–261, Oct. 1999.

[63] S. Cakir and A. E. Cetin, "Mel-Cepstral Feature Extraction Methods for Image Representation," *Optical Engineering*, vol. 49, Sept. 2010.

[64] O. Yorulmaz, T. C. Pearson, and A. E. Cetin, "Detection of Fungal Damaged Popcorn Using Image Property Covariance Features," *Computers and Electronics in Agriculture*, vol. 84, pp. 47–52, Jun. 2012.

[65] N. Kingsbury, "The Dual-Tree Complex Wavelet Transform: A New Technique For Shift Invariance And Directional Filters," in *8th IEEE DSP Workshop*, pp. 319–322, Aug. 1998.

[66] I. W. Selesnick, "Hilbert Transform Pairs of Wavelet Bases," *IEEE Signal Processing Letters*, vol. 8, pp. 170–173, Jun. 2001.

[67] N. Kingsbury, "A Dual-Tree Complex Wavelet Transform with Improved Orthogonality and Symmetry Properties," in *International Conference on Image Processing*, vol. 2, pp. 375–378, Sept. 2000.

[68] N. Kingsbury, "Image Processing with Complex Wavelets," *Philosophical Transactions of the Royal Society of London*, vol. 357, pp. 2543–2560, Sept. 1999.

[69] A. Yazar, F. Keskin, B. U. Toreyin, and A. E. Cetin, "Fall Detection Using Single-Tree Complex Wavelet Transform," *Pattern Recognition Letters*, 2012. Available online 28 December 2012.

[70] F. Keskin and A. E. Cetin, "Time-Varying Lifting Structures for Single-Tree Complex Wavelet Transform," in *IEEE 20th Signal Processing and Communications Applications Conference (SIU-2012)*, Apr. 2012.

[71] F. Keskin, A. Suhre, and A. E. Cetin, "Single-Tree Complex Wavelet Transform via Time-Varying Lifting Structures." submitted to 20th European Signal Processing Conference (EUSIPCO-2012), 2012.

[72] J. K. Romberg, H. Choi, R. G. Baraniuk, and N. Kingsbury, "A Hidden Markov Tree Model for the Complex Wavelet Transform," in *IEEE Transactions on Signal Processing*, pp. 133–136, 2001.

[73] E. B. Soyer, "Pyroelectric Infrared (PIR) Sensor Based Event Detection," Master's thesis, Bilkent University, 2009.

[74] A. Yazar, B. U. Toreyin, and A. E. Cetin, "Human Activity Classification Using Vibration and PIR Sensors," in *IEEE 20th Signal Processing and Communications Applications Conference (SIU-2012)*, pp. 1–4, Apr. 2012.

[75] A. Yazar and A. E. Cetin, "Ambient Assisted Smart Home Design Using Vibration and PIR Sensors," in *IEEE 21st Signal Processing and Communications Applications Conference (SIU-2013)*, pp. 1–4, Apr. 2013.

[76] C.-C. Chang and C.-J. Lin, "LIBSVM: A Library for Support Vector Machines," *ACM Transactions on Intelligent Systems and Technology*, vol. 2, no. 27, pp. 1–27, 2011.

[77] Fastcom Technology SA, "Method and Device for Detecting Fires Based on Image Analysis," Application Notes No. WO02/069292, PCT Publication, 2002.